M.Sc. Thesis
Master of Science in Engineering

DTU Electrical Engineering
Department of Electrical Engineering

HVDC Control And Operation For The Integration Of Extremely High-RES Systems

With Focus On Permanent DC Faults

Ona Renom Estragues

Kongens Lyngby 2019

DTU Electrical Engineering
Department of Electrical Engineering
Technical University of Denmark

Ørsteds Plads
Building 348
2800 Kongens Lyngby, Denmark
Phone +45 4525 3800
elektro@elektro.dtu.dk
www.elektro.dtu.dk

Summary

This master thesis presents the control and analysis of a DC fault on a zero inertia offshore grid integrating multiple Voltage Source Converters. The system analyzed consists in an offshore grid which includes two wind power plants and two offshore converter platforms. These two offshore converter platforms are connected to two different onshore grids through High Voltage Direct Current (HVDC) point-to-point connections.

First, the modeling and control of Voltage Source Converters for offshore wind energy HVDC systems are presented. Two control strategies are described for them depending on their operating mode which can be grid-forming or grid-following.

Then, the complete model of the system, including the onshore grids, is presented. For simulation purposes an aggregated model is used for the WPPs. Further, two control methods for power reduction for the system to be able to perform correctly under DC faults are proposed.

Finally, a simulation of the modelled system under a pole-to-pole DC fault on one of the HVDC transmission links is performed and evaluated by means of time domain simulations using Matlab Simulink®.

Preface

This Master Thesis was prepared at the department of Electrical Engineering at the Technical University of Denmark (DTU) in fulfillment of the requirements for acquiring a M.Sc degree in Industrial Engineering from The Politechnical University of Catalunya (UPC). This thesis was conducted during the spring semester of 2019 and it corresponds to 30 ECTS points. It has been carried out under the supervision of Spyros Chatzivasileiadis and Georgios Misyris.

Kongens Lyngby, July 4, 2019

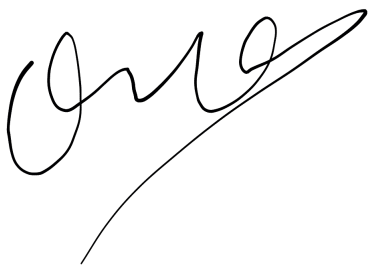

Ona Renom Estragues

Acknowledgements

Firstly I would like to thank my supervisors Spyros Chatzivasileiadis and Georgios Misyris for giving me the opportunity of performing my Master thesis on HVDC technology. The guidelines and supervision of Spyros have been essential for the development of this work. Special thanks go to Georgios for the support received with the technical areas of the project and for the time dedicated to resolving different doubts. The knowledge that I have acquired during these months would have been much less without his supervision and support. I would also like to thank Eduardo Prieto from CITCEA-UPC for introducing me to the HVDC technology a few years ago and for being available for little discussions during these five months.

Also, I would like to thank my roommates from G0 for the family environment created during my stay here at DTU. You made it very easy to love the experience within the first week.

From back home I owe many thanks to Íngrid and Ricard for their support and help both in the technical and motivational aspects. You have been my motivation boost when I needed it the most and without you, this thesis would not have been possible. Also, I would like to thank Luis for sharing the experience of doing a Master Thesis abroad exchanging songs exchange and having nice conversations.

Finally I would like to thank my mum. Moltes gràcies mama, se que ho saps, però sense tu no hauria arribat fins aquí ni hauria aconseguit tant. Nose si t'ho dic suficient però els teus ànims m'han ajudat tirar endavant en els pitjors moments i alegrat cada dia. T'estimo.

Contents

List of Figures

List of Tables

Acronyms

ACCB AC Circuit Breaker. 31, 44, 52–54

AVC Alternating-Voltage controller. 22, 23, 36, 49, 50

AVM Averaged-value Model. 12–14, 18

CLC Current-Limitation Controller. 49

EMT Electromagnetic Transient. 11

GSC Grid Side Converter. vii, ix, xi, 6, 11, 19, 20, 29, 34–37, 50, 51

HVAC High Voltage Alternate Current. 2, 6–8

HVDC High Voltage Direct Current. i, ix, xi, 1–3, 6, 8, 9, 11, 18, 25, 28–31, 34, 35, 39, 44–47, 49, 53, 55, 57, 58

IGBT Insulated-gate bipolar transistor. 8, 9, 32, 47, 57

LPF Low-pass filter. 36, 50

MMC Modular Multilevel Converter. 9, 12

MSC Machine Side Converter. 6, 11, 19

MTDC Multi terminal DC. 8

NSWPH North Sea Wind Power Hub. 1, 5, 7, 26, 58

PCC Point of Common Coupling. 14, 16

PI Proportional-Integral. 17, 19, 28, 31, 38

PLL Phase-Locked Loop. 15, 16, 18, 20–22, 36, 37

PMSG Permanent Magnet Synchronous Generator. ix, 11, 33

PSL Power Synchronization Loop. 22, 23, 36

PWM Pulse Width Modulation. 8

RES Renewable Energy Resources. 1

SRF Synchronous Reference Frame. 12, 17

SVPWM Space Vector PWM. 8

TSO Transmission System Operators. 1

UNFCCC United Nations Framework Convention on Climate Change. 1

VSC Voltage Source Converter. vii–ix, xi, 3, 5, 8–20, 22–30, 32, 34–36, 38–47, 49–54, 57, 58

WPP Wind Power Plant. i, ix, 2, 5–8, 11, 25, 28–31, 33, 37, 39–41, 44, 47, 50, 52–54, 57

WT Wind Turbine. vii, ix, xi, 5, 6, 11, 19, 20, 29, 34–37, 50, 51

WTG Wind Turbine Generators. 11

CHAPTER 1

Introduction

In this chapter, the background and motivation for the execution of the present master thesis are described. Moreover, the goal sought to pursue with this work is defined. Furthermore, the methodology followed to reach this goal is briefly explained. Finally, the structure of the thesis, including an overview of the content of each chapter, is presented. This content will be further developed in the next chapters.

1.1 Context and Motivation

Nowadays climate change has become one of the world's main issues, especially due to global warming which causes from change in the weather patterns to the rising of the sea level. Regarding this problem and to keep global warming below 2°C, parties of the United Nations Framework Convention on Climate Change (UNFCCC) signed the Paris Agreement in 2015 [1], promoting, among other actions, the investment in Renewable Energy Sources (RES) in order to replace the actual fossil fuel-based Energy Production and reduce greenhouse gases emissions.

Within this framework, the North Seas Countries have also signed a political declaration on energy cooperation to improve conditions for the development of offshore wind energy [2]. Regarding this development and in order to achieve the objectives set by 2040, an innovative solution has been proposed with the support of Dutch, Danish and German Transmission System Operators (TSOs). This solution consists on the creation of the North Sea Wind Power Hub (NSWPH), an artificial island located in the north sea integrating up to 30 GW of offshore wind power generation [3], [4]. In addition to the integration of the power of thousands of offshore Wind Turbines, this NSWPH would have multiple connections to five different countries: Germany, Netherlands, UK, Denmark and Norway; benefiting from an internationally coordinated roll-out scenario which has the potential to reduce the cumulative cost of the transmission infrastructure [5]. In order to build this North Sea Wind Power Hub several technical studies must be carried out for the island grid and its connections to land. These studies are part of the multiDC project, a project which goal is to develop innovative methods for the optimal coordination of multiple HVDC lines and HVDC grids in systems with high shares of renewables [6].

Since this artificial island would be located in the north sea far from shore, its connection to the different onshore grids would be based on point to point connections using High Voltage Direct current (HVDC). Yet, the configuration of the island grid or the hub connecting the different offshore wind power plants to the different HVDC links to shore, can either be in HVDC or High Voltage Alternate Current (HVAC), both presenting different challenges. In the case of an HVDC configuration for the offshore grid, DC circuit breakers would be required to isolate DC faults, increasing the cost of the overall system [7]. On the other hand, the use of an HVAC grid for the interconnection of the offshore system would involve having zero inertia grid on the island, challenging the stability of the system [8], [9].

The scope of the work included in this report is intended to be part of the multiDC project, mentioned previously in this section, with the aim to create a small-scale representative non-linear simulation model of the island system and in order to test some faults and study its stability. The model will be formed by the island grid, multiple Wind Power Plant (WPP)s and two HVDC transmission lines to shore. In addition, it will include three different power converters: WPP converters, the offshore converters and the onshore converters. In particular, this thesis will be focused on the impact of having a zero inertia system on the island grid with power converters acting as generators setting the reference voltage and frequency of it. Moreover, this thesis main objective is to develop a control methodology to maintain the stability of the Zero inertia system after an event of a DC fault and further disconnection of one of the HVDC transmission lines. This control methodology will be based on power reduction of the WPP with two main focus: reduce the generated power to the system's maximum export capability and to restore the connected HVDC transmission line power to its pre-fault value.

1.2 Methodology of this Thesis

This thesis will focus on the study of a permanent DC fault considering a zero inertia system. For this purpose, a nonlinear Simulation model will be created and the Simscape package of Matlab-Simulink®is chosen to be the Simulation Software to develop this model. Moreover, this simulation model will be composed of different elements such as Onshore, Offshore and wind turbine converters, transformers, lines... At the same time, different control approaches will have to be defined in order to achieve stability and a well-performance on the AC offshore grid under a DC fault.

Regarding the simulation model, for easier implementation of it, this model will be split into different parts. Firstly a simulation model of each type of converter and their different control strategies will be implemented. Each of this control strategies will be formulated based on existing techniques found in the literature. Once the three simulation models are working, they will be merged including other elements such as transformers and lines. Finally, a simulation system composed of two converters of each type, having two HVDC point to point connections to shore and two wind farms, connected through a zero inertia offshore grid.

Looking into the control design, first, a control strategy will be designed for each of the three types of converters. Since the model will have an offshore grid including multiple wind farms and transmission lines, a control approach for the power flow will be defined. This control will be based on droops on the active power in the offshore VSC converters. Finally, a functional model for steady state operation will be achieved. Yet, this model will not behave properly under a DC fault case scenario.

For achieving a model suitable for testing DC faults, more control strategies will need to be designed. First, the operating limits of the different converters need to be taken into account. For this reason, current and voltage limiting current strategies will be designed and incorporated in the different converter controls. Furthermore, two power reduction control strategies will be implemented. A first control strategy will consist on reducing the power injection of the wind turbines to the maximum export capability of the system in order to maintain the stability once the converter limits are reached. A second slower control strategy will be designed in order to achieve the pre-fault state by means of power balance. Finally, both strategies will be combined.

These different control strategies will be incorporated into the model and different simulations will be performed in order to verify if a correct behaviour is achieved during a permanent DC fault followed by an outage of one of the transmission lines.

1.3 Structure of the Thesis

This thesis is divided in six chapters as follows:

- Chapter 2 provides a literature review about Offshore Wind Power Energy and HVDC Technology. It presents relevant research topics for the scope of this master thesis. It describes from the basic configuration of an Offshore Wind Power Plant connected to shore to DC faults and its effects on the stability of AC systems.
- Chapter 3 focuses on Voltage Source Converter (VSC). First, the Averaged Voltage Source Converter model considered for the studies is presented. Further, the three types of Voltage Source Converters of the study system are described, detailing the electrical configuration of the systems and their control strategies.
- Chapter 4 analyzes a communication-based control method for power reduction on the study system formed by an offshore AC grid which integrates two Wind Power Plants and two HVDC based transmission systems to shore. This power reduction control is based on the principle of restoring the pre-fault equilibrium values on one HVDC transmission links after a DC fault occurs in the other HVDC links. Firstly, the power sharing control strategy when having two offshore VSCs connected in parallel is introduced. Further, additional controls such as the operational limits for the onshore converters and different protection systems are also described. Finally, a test system is set up and these control approaches are analyzed through different case studies.

- Chapter 5 describes another control methodology for power reduction under a permanent DC fault, on the same system as Chapter 4, based on the maximum power transfer capability of the offshore converters using the AC voltage of the offshore AC grid as a control signal. Further, the additional controls described in Chapter 4 are also considered in this Chapter and the operational limits for the offshore converters are introduced. Finally, studies are performed on this methodology, including one based on the combination of this technique with the power reduction method from Chapter 4.
- Chapter 6 summarizes the results and concludes the thesis, providing suggestions on future work to improve the simulation model and regarding the study on this zero inertia system.

CHAPTER 2

Offshore Wind Energy and HVDC Technology

This chapter focuses on offshore wind energy and the current state-of-art of the technologies considered for this master thesis. Further, the main grid connection options for offshore Wind Power Plants (WPPs) including the NSWPH approach are described. Finally, two VSC technologies alongside with the main impacts of a DC fault on an AC offshore system are introduced.

2.1 Introduction to Offshore Wind Power Plants

2.1.1 Wind Turbines Technology for WPPs

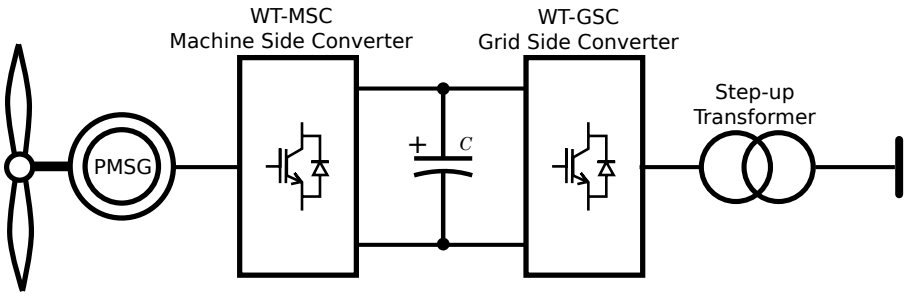

Figure 2.1: Permanent magnet synchronous machine with Full-scale converter Wind turbine

Different types of Wind turbines for WPPs are described in the literature [10], [11]. However, for Offshore wind energy applications, WT with full-scale converter is broadly used. This type of wind turbine technology also referred to as type 4 wind turbine model, can be divided into a mechanical and electrical sub-system. The first one enfolds the drive-train and the generator. For most applications, the generator used is a permanent magnet synchronous generator in which, in some cases, the gearbox can be omitted (direct-driven PMSG) [12], [13]. Further, regarding the electrical part, this type of WT consists of a full-scale converter. As shown in 2.1, the full-scale converter is based on a back-to-back configuration for interconnecting the mechanical part with the electrical

grid. This back-to-back configuration couples the WT-MSC with the WT-GSC through a DC link. This link decouples both sides in terms of frequency, voltage and reactive power since the DC link only transmits active power.

2.1.2 Offshore WPPs connection to onshore grids

Figure 2.2 shows different offshore wind grid connection concepts described in [5] and [14]. When the distance of the WPP to mainland small (less than 80 km), the left configuration of Figure 2.2 is selected. In this configuration, the WPP includes an offshore 220 kV HVAC platform which is connected to the mainland through an HVAC link. Further, when the distance to shore is increased above 100 km, HVDC technology is used to connect the differentWPPs to the mainland. In this situation HVAC connections become cumbersome due to reactive power compensation and reducing the active capability and HVDC becomes a more cost-effective solution. In this case the offshore platform includes HVDC converters.

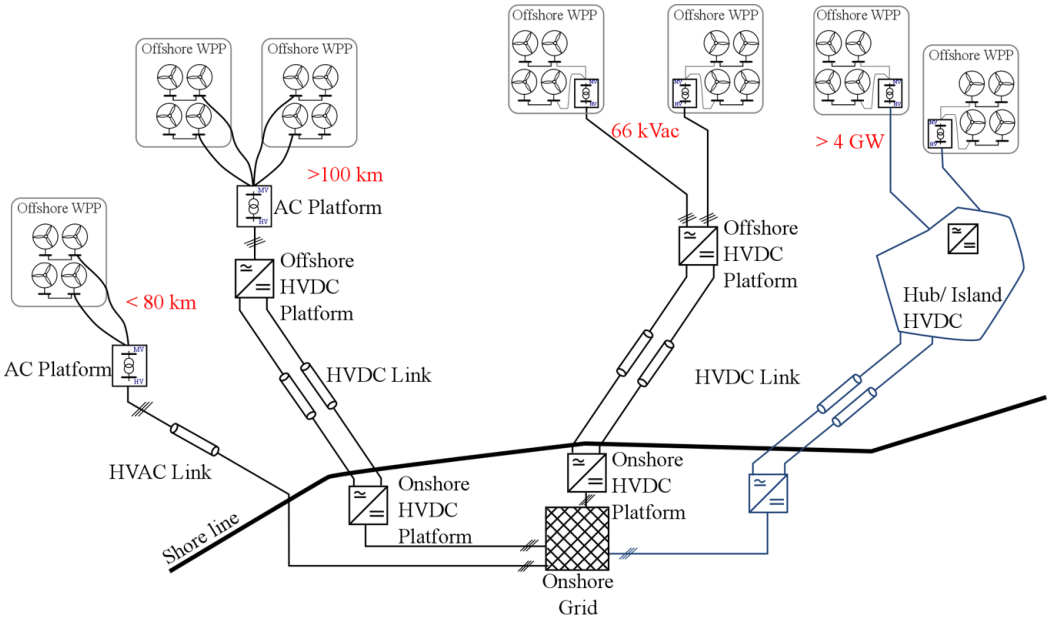

Figure 2.2: Offshore WPPs connection to main grid

There are two options regarded for connecting the WPPs to this offshore platform :

- connecting first the WPP to an AC collector platform that includes a step-up transformer which steps up the voltage from a medium voltage level to voltage level (often 150 kV). Then this AC platform is connected through a HVAC line to the offshore platform reducing the transmission losses. This corresponds to the second left configuration in Figure 2.2.
- connecting directly the WPP at a 33 kV or a 66 kV level to the offshore platform creating cost benefits over the AC collector. However, this option is limited for wind farms with a power capability inferior to 4 GW. This option corresponds to the third configuration represented in Figure 2.2.

When having large wind farms with a power capability above 4 GW an innovative concept consisting of transporting the power to a hub is introduced. This concept is introduced by the NSWPH and corresponds to the configuration on the right in Figure 2.2.

2.1.2.1 North Sea Wind Power Hub Approach

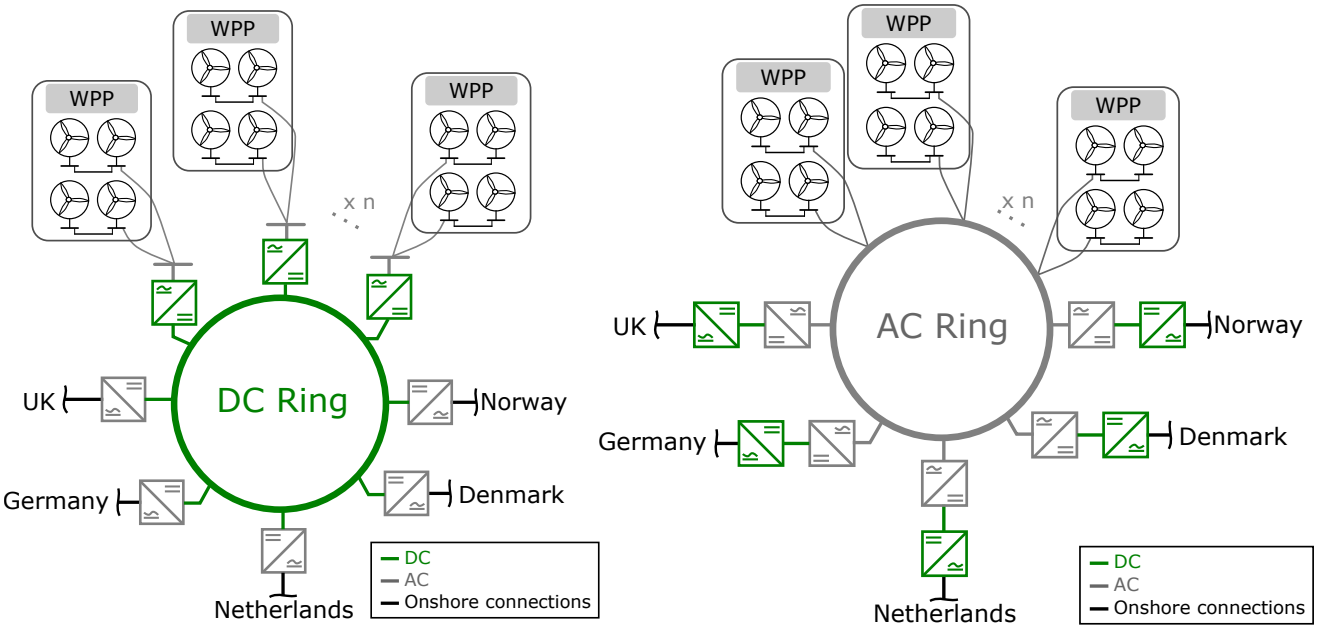

(a) DC Ring (b) AC Ring

Figure 2.3: Island Hub configurations

The North Sea Wind Power Hub consists of an artificial island connecting multiple WPPs to different countries. This island approach can facilitate power conversion and storage to support short and long term flexibility options to the grid and allows to optimize the overall cost of offshore assets [4], [5].

An AC configuration for the island grid leads to an AC ring that connects the different WPPs with different HVDC transmission links connecting to shore as shown in Figure 2.3b is considered in this project. However,a DC configuration for the island grid derives to having a DC ring connecting the different countries to multiple WPPs as shown in Figure 2.3a is also an option. In the first scenario, the WPPs are connected to the island grid through HVAC cables whereas for a DC ring, these connections are done through HVDC. Furthermore, in the AC ring configuration, the connections to shore are done using HVDC point-to-point connections while with a DC configuration the case of multi-terminal DC (MTDC) grid is addressed.

2.2 VSC converters for HVDC

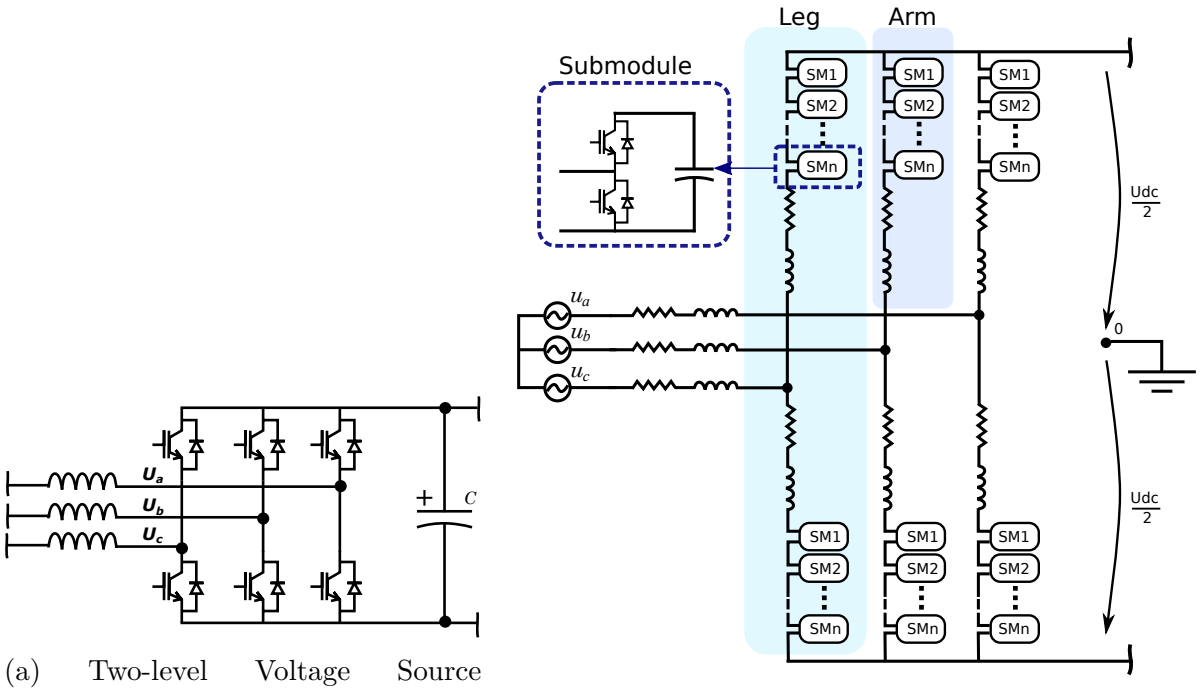

(a) Two-level Voltage Source Converter scheme

(b) Modular Multilevel Converter scheme

Figure 2.4: Voltage source converter schemes

Voltage source converters receive this name since they act as a voltage source. These converters allow the power transfer from AC to the DC side and vice versa. VSCs are composed of three legs or branches (one for each AC phase) and six arms (one for each leg). Each of these arms contains multiple insulated-gate bipolar transistors (IGBTs) which are their turn-off and turn-off can be controlled by using PWM techniques, being Space Vector PWM (SVPWM) the most widely used modulation Technique [15]. There exist different types of VSC converters classified by the voltage levels the output voltage is switched. The most common ones are:

- **Two-level VSC**: This converter, shown in Figure 2.4a is the simplest type of Voltage Source Converter [16]. Each arm of the converter is composed of multiple IGBT connected in series which must be switched simultaneously. As the name implies, the AC output of each phase is switched between two voltage levels: $-\frac{1}{2}\,U_{dc}$ and $+\frac{1}{2}\,U_{dc}$.
- **Modular Multilevel Converter (MMC)**: This type of converter was first proposed in 2003 and has become the best option for VSC converters for HVDC [17]. In this converter, each arm is composed of multiple identical sub-modules connected in series. These sub-modules are individually controlled and have their own capacitive storage becoming, each of them, two-level half-bridge converters. The series connection of the sub-module allows the AC output of each phase to have multiple levels, being the generated AC signal wave-form similar to a sin-wave. This implies a lower harmonic content than the Two-level VSC. One of the main disadvantages of this type of converter relies on the complexity of its control [12], [18]. The MMC scheme is represented in Figure 2.4b.

2.3 DC Faults in Offshore HVDC systems

The impact of DC faults on an AC offshore grid depends on the topology of the AC and DC systems, the fault type and the employed protections [19]. Considering an HVDC point-to-point topology, a DC fault will always imply a permanent loss of power transfer to the onshore grid which might lead to the loss of synchronism of the offshore grid converters and generators [19]. To avoid this situation, the maximum power injection is defined to maintain the frequency within boundaries [19].

Furthermore, grid protection is required to minimize the DC fault impact on the onshore and offshore networks and to minimize the stress to components [20]. For systems with HVDC point-to-point topology, AC circuit breakers can be used instead of DC breakers, reducing the system economic cost [7]. As described in [19], under a DC contingency, such as a DC transmission line fault, two AC breakers are located on the AC side of each converter terminal open, isolating the fault from both AC girds. This operation takes from 40 to 80 ms after the fault is detected [19], [20].

At the same time, the IGBT's of the affected converters are blocked to prevent over-currents. In these situations, the current is now flowing through the free-wheeling diodes as shown in Figure 2.5. Thus, the blocked converter acts as a current source to the DC side and the remaining offshore-VSC converter is now setting the frequency of the offshore network by itself.

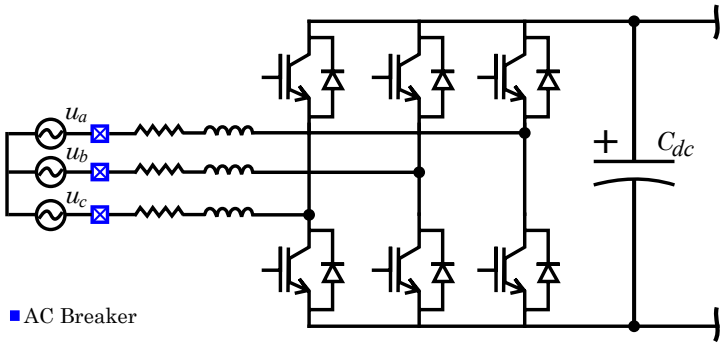

(a) Two-level VSC scheme

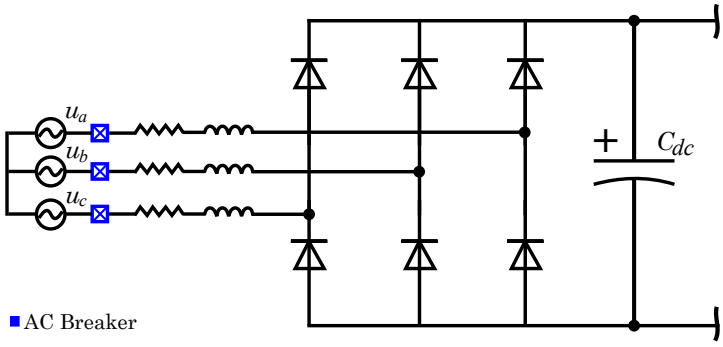

(b) Blocked VSC scheme

Figure 2.5: Scheme of converter blocking

CHAPTER 3

Control of VSC converters for Offshore Wind Energy

This Chapter gives an introduction to VSCs dynamic modeling and the control strategies used for the development of this thesis. First, the model conventions used are introduced. Secondly, the Voltage Source converter Averaged Model is presented. Next, the different control strategies applied in the system of study depending on the VSC operational mode are described. The control strategies described in this Chapter are the ones used in the Dynamic EMT simulations case studies presented later in Chapter 5.

3.1 Introduction

The Wind Generation system of WPP commonly consists of Full-converter Wind Turbine Generators (WTGs) using Permanent Magnet Synchronous Generators (PMSG). However, when studying large WPPs, aggregated models are often used in the dynamic simulations for representing the dynamics of the wind turbines, reducing the size of the system [21], [22]. Furthermore, these aggregated models neglect the mechanical behavior of the wind turbines and the machine side converters (MSCs) substituting them by controlled current sources.

Apart from the Wind Turbine Grid Side Converters (GSC) connecting the WT with the offshore grid, Offshore WPPs include Offshore and Onshore VSC connected through a point to point HVDC link. These different VSCs differ in their control approaches depending on their operating principle and the input signals on their control system. Based on the operating principle VSCs can be classified in grid-Following (also called grid-supporting) or grid-Forming [23]. Under this nomenclature, the operation of the WPP VSCs considered on this work is defined as:

- **WT - GSC**: operate in grid-following mode where they balance the voltage of the DC wind turbine link and control the reactive power exchange with the offshore grid at the LC filter.
- **Onshore - VSC**: operate in grid-following mode and control the DC voltage of the HVDC link and the reactive power exchange with the main grid.
- **Offshore - VSC**: operate in grid-forming mode and control the AC voltage magnitude and the frequency of the offshore grid.

3.2 Model conventions

For the conduct of this work, transformations are applied to different quantities of the system. These transformations have been used to simplify either the control strategy or the mathematical and computational analysis.

Firstly, the per-unit system methodology is applied frequently to the electrical values of the system. When these values are defined by upper case letters they correspond to the physical quantities while when they are represented by lower case letters they correspond to the quantities in the per-unit system. The per-unit system base values used in this thesis are presented in Appendix A.

Furthermore, as the quantities in the stationary three-phase *abc*-reference frame in an electrical AC system are not stationary but nonlinear time-variant functions, a transformation into a synchronous reference frame (SRF) is sought. The quantities expressed in the SRF are not time-dependent and are constant values, without an oscillatory behavior, unless a disturbance is applied to the system. The SRF is achieved by applying the dq0 transform, detailed in the Appendix B.1, on the different quantities of the system. The d-axis of *dq*-frame is aligned with the measured voltage at the corresponding filter capacitor and the q-axis is leading the d-axis by 90º. In this frame, the *d*-component will be designated as real and the *q*-component as imaginary in the complex plane (3.1), whereas the third component is always 0.

$$x_{dq} = x_d + jx_q \tag{3.1}$$

3.3 Averaged Model Voltage Source Converter

For dynamic simulation purposes, the different types of VSC converters can be modelled as averaged models. Several Averaged Models (AVMs) have been proposed to represent accurately the behavior of these converters in dynamic simulations [18], [24]. Although the averaged model of an MMC-VSC presented in [12] is more detailed, in this thesis a less complex model is implemented for all the converters due to the number of the converter required in the study system. The averaged model of a two-level VSC described in [25] is used which can reproduce the dynamic performance with sufficient accuracy. In this simplification, the AC side of the converter is represented as three ideal controlled voltage sources, U_l, where the DC side is modelled as a controlled current source, I_{dc}, as shown in Figure 3.1.

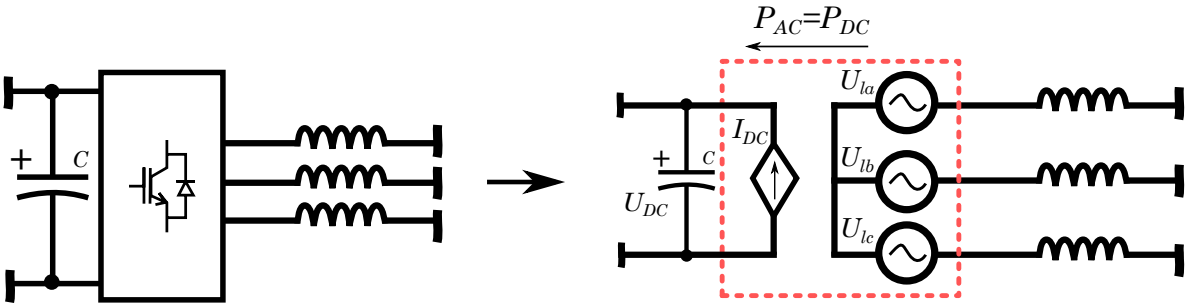

Figure 3.1: VSC converter averaged model

The controlled voltage sources of the AVMVSC are expressed as:

$$\begin{aligned} U_{la} &= \frac{1}{2} U_{refa} U_{DC} \\ U_{lb} &= \frac{1}{2} U_{refb} U_{DC} \\ U_{lc} &= \frac{1}{2} U_{refc} U_{DC} \end{aligned} \tag{3.2}$$

In which U_{refa}, U_{refb} and U_{refb} are the output voltages obtained from the control system. This voltages are defined by:

$$\begin{aligned} U_{refa} &= m_a \sin(\omega t + \delta) \\ U_{refb} &= m_b \sin(\omega t + \delta - \frac{2\pi}{3}) \\ U_{refc} &= m_c \sin(\omega t + \delta + \frac{2\pi}{3}) \end{aligned} \tag{3.3}$$

Where δ is the phase angle of the output voltage and m_a, m_b, m_c are the modulation indexes of each phase, defined as the ratio between the maximum fundamental peak phase voltage and the DC voltage.

In this averaged model the switching commutations are not represented so there is a nonexistent harmonic content in the voltage and current value. Considering a balanced system and neglecting the converter loses, the power from the AC side is equal to the Power of the DC side. Under this consideration, the I_{DC} is expressed as:

$$I_{DC} = \frac{P_{AC}}{U_{DC}} = \frac{1}{2}\Big(U_{refa} I_a + U_{refb} I_b + U_{refc} I_c\Big) \tag{3.4}$$

3.4 Grid-following converter control

A basic structure of a grid-forming connected VSC and its control structure is shown in Figure 3.2. Regarding the electrical configuration of the grid-following converters substations, it includes an AVM VSC converter which on the AC side is connected to the point of common coupling (PCC) through a series reactance. Often this reactance corresponds to an AC filter, either an LC or and LCL type and is introduced to filter the harmonic content originated at the output of the converter. For this study, an LC filter has been considered. Additionally, a transformer can be added after the LC filter to step up the voltage up to the grid level. On the DC side, these converter stations include a DC capacitor to help maintain the DC voltage at the operating limits.

Further, regarding the control system, this topology is based on the well-known vector control [15], [21]. In this control method, the $dq0$ transform is used in order to work with constant magnitudes. The control structure is shown in Figure 3.2 consists on a cascade control formed by an outer and an inner controller. The outer controller takes as an input the measured signals of the electrical system and calculates the current references which are given as an input to the inner controller, also called current controller and generates the reference modulation signal for the converter.

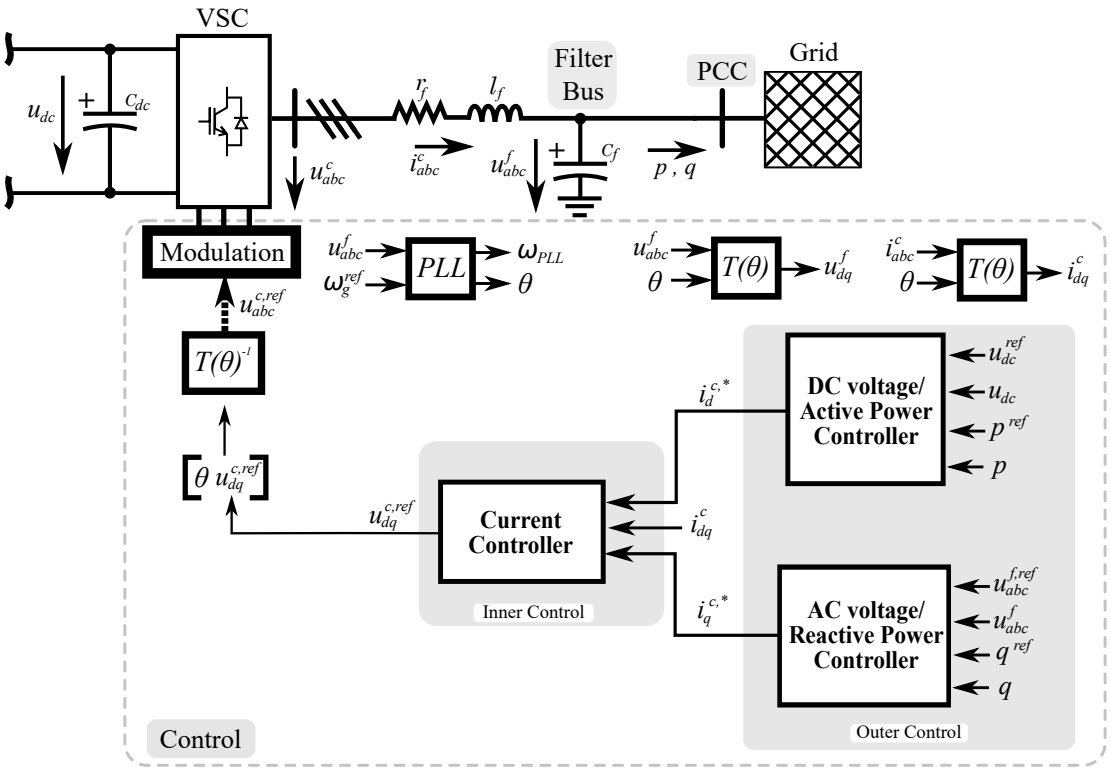

Figure 3.2: Schematic of cascade control for Grid-following converters

Another important element present in the grid-following converters is the Phase-Locked Loop. This element functionality is to synchronize the converter to the AC grid voltage angle measured at the capacitor filter. More precisely, the PLL tracked angle is the one used as the reference rotating angle in the $dq0$ Transform.

3.4.1 Onshore converter

The Onshore-VSC system and its control approach is detailed in Figure 3.3. As mentioned before, it contains a PLL, an inner current controller and two outer controllers: a reactive power controller and a DC voltage controller. Although there is a wide range of techniques presented for the vector control of these converters in the literature, the outer controllers are modelled following the methodology described in [26] whereas the inner controller and the PLL are modelled using [27] as a reference. The different control loops and the system differential equations are presented in the following subsections.

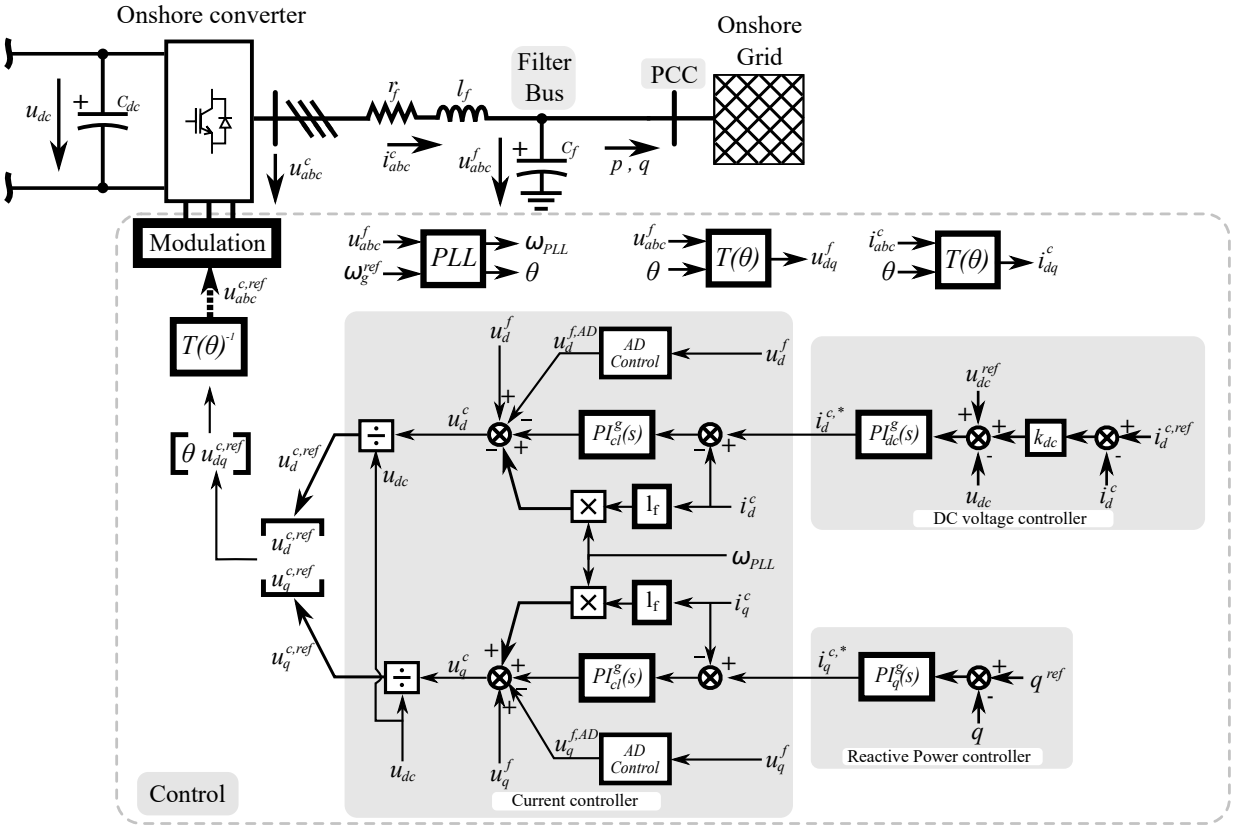

Figure 3.3: Onshore-VSC control scheme

3.4.1.1 Phase-Locked Loop

The PLL synchronizes the grid-following converters to the corresponding AC networks. It provides an estimation of the frequency (ω_{PLL}) and the angle (θ_{PLL}) of the grid. The synchronization of the converter is achieved by aligning the d-axis of the internal reference frame with the space vector of measured voltage at the capacitance filter or the PCC (u^f).

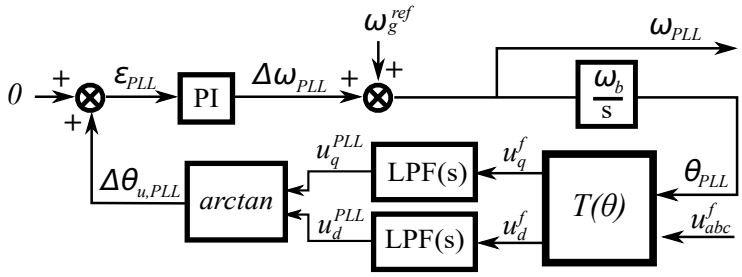

Figure 3.4: Phase Locked Loop

The PLL design used in this study is shown in Figure 3.4. This uses an inverse tangent function on the low-pass filtered dq-components of the measured voltage at capacitor filter (u_{dq}^{PLL}) to approximate the phase angle error. Then, a PI controller is applied to this error to estimate the frequency of the grid, ω_{PLL}. Finally, this frequency is converted into real quantities and integrated the obtaining the tracked grid angle, θ_{PLL}. This procedure is described in the Laplace domain by the following equations:

$$\epsilon_{PLL} = \Delta\theta_{u,PLL} = \arctan\left(\frac{u_{PLL,q}}{u_{PLL,d}}\right) \tag{3.5}$$

$$\Delta\omega_{PLL} = \left(k_{p,PLL} + \frac{k_{i,PLL}}{s}\right)\epsilon_{PLL} \tag{3.6}$$

$$\Delta\theta_{u,PLL} = \frac{\omega_b}{s}\Delta\omega_{PLL} \tag{3.7}$$

$$\omega_{PLL} = \Delta\omega_{PLL} + \omega_g \tag{3.8}$$

$$\Delta\theta_{PLL} = \frac{\omega_b}{s}\omega_{PLL} \tag{3.9}$$

Where $k_{p,PLL}$ and $k_{i,PLL}$ are the proportional and integral gains. $\Delta\omega_{PLL}$ and $\Delta\theta_{u,PLL}$ are the angular velocity and phase angle deviation of the PLL with respect to the grid values. Finally, ω_g and ω_b correspond to the reference grid and the base frequency values respectively.

The transfer function of first order low-pass filters showed in Figure 3.4 is given by:

$$LPF(s) = \frac{\omega_{LP,PLL}}{s + \omega_{LP,PLL}} \tag{3.10}$$

With $\omega_{LP,PLL}$ is the cut-off frequency of the LPF.

3.4.1.2 Inner Current Controller

The inner current control structure is shown in Figure 3.3. The objective of this controller is to maintain the current flowing through the phase reactor, i^c_{abc}, at the reference value. For the design of the inner current controller, the differential equations of the AC system are considered. Assuming the LC filter as an interface of the VSC and the grid, the per-unit phase voltage and currents are given by:

$$\frac{l_f}{\omega_b}\frac{di^c_{abc}}{dt} + r_f i^c_{abc} = u^c_{abc} - u^f_{abc} \tag{3.11}$$

Where ω_b is the base angular frequency, l_f and r_f are the filter inductance and resistance, u^c_{abc} is the output voltage of the converter, u^f_{abc} is the voltage at the filter capacitance and i^c_{abc} is the current flowing from the converter to the Filter bus.

At the same time, equation (3.11) can be expressed in the SRF using the component form as:

$$\begin{aligned} \frac{l_f}{\omega_b}\frac{di^c_d}{dt} + r_f i^c_d - l_f\omega_{PLL} i^c_q = u^c_d - u^f_d \\ \frac{l_f}{\omega_b}\frac{di^c_q}{dt} + r_f i^c_q + l_f\omega_{PLL} i^c_d = u^c_d - u^f_q \end{aligned} \tag{3.12}$$

In (3.12) it can be seen that the d-component and q-component are coupled by the cross terms of $\omega_{PLL} l_f i_d$ and $\omega_{PLL} l_f i_d$. However the control system requires a decoupled control of i_d and i_q. This is achieved by using a feed-forward controller. Using (3.13) and substituting them in (3.12), the decoupled system in (3.14) is obtained. Once this two components are decoupled, a conventional SRF control structure using PI controllers can be applied to the decoupled system described in the Laplace domain by (3.15).

$$\begin{aligned} u^c_d = u^f_d - \omega_{PLL} l_f i_q + u^d_d \\ u^c_q = u^f_q + \omega_{PLL} l_f i_d + u^d_q \end{aligned} \tag{3.13}$$

$$\begin{aligned} u^d_d = \frac{l_f}{\omega_b}\frac{di^c_{dq}}{dt} + r_f i^c_{dq} \\ u^d_q = \frac{l_f}{\omega_b}\frac{di^c_q}{dt} + r_f i^c_q \end{aligned} \tag{3.14}$$

$$u^d_{dq} = \left(k^g_{p,cl} + \frac{k^g_{i,cl}}{s}\right) \cdot (i^{c,*}_d - i^c_{dq}) \tag{3.15}$$

In (3.15) $k^g_{p,cl}$ and $k^g_{p,cl}$ represent the proportional and integral gains of the PI controller, $PI^g_{cl}(s)$, tuned using the Modulus Optimum criterion described in [28].

Finally, the output voltage reference resulting from the current controller, u^c_{dq} is defined according to (3.16). Substituting (3.14) in (3.16) the complete expression of u^c_{dq} (3.17) is obtained.

$$\mathbf{u}_{dq}^{c} = u_{dq}^{d} + j \cdot l_f \cdot \omega_{PLL} \cdot \mathbf{i}_{dq}^{c} + \mathbf{u}_{dq}^{f} - \mathbf{u}_{AD}^{*} \tag{3.16}$$

$$\mathbf{u}_{dq}^{c} = PI_{cl}^{g}(s) \cdot \left(\mathbf{i}_{dq}^{c,*} - \mathbf{i}_{dq}^{c}\right) + j \cdot l_f \cdot \omega_{PLL} \cdot \mathbf{i}_{dq}^{c} + \mathbf{u}_{dq}^{f} - \mathbf{u}_{AD}^{*} \tag{3.17}$$

An additional term is added to the control structure to suppress the LC oscillations of the filter. The oscillations are first isolated by a low-pass filter and then multiplied by a gain. The result is the term u_{AD}^{*} which is added to the reference output voltage reference, u_{dq}^{c}. This active damping is described in the Laplace domain by the following equations:

$$u_{AD} = k_{AD}(u_{dq}^{f} - \phi) \tag{3.18}$$

$$\phi = \frac{\omega_{AD}}{s + \omega_{AD}} \cdot u_{dq}^{f} \tag{3.19}$$

Where ω_{AD} is the cut-off frequency of the low pass filter.

3.4.1.3 Outer Controllers

The outer controllers are used to obtain the reference dq current values, $i_{dq}^{c,*}$, for the inner controller. These outer loops regulate the current reference is through the measured voltage or power signals. This outer controller must be around ten times slower than the inner controller to maintain the stability on the system [15]. According to the Instantaneous Power Theory, the active and reactive per-unit power in the $dq0$-reference frame is defined by [29]:

$$p = u_d i_d + u_q i_q \tag{3.20}$$

$$q = u_q i_d - u_d i_q \tag{3.21}$$

Furthermore, knowing that the PLL aligns the measured voltage at the filter capacitance with the d-axis, the q-component of this voltage is equal to zero, $u_q^f = 0.0$ p.u. With this consideration equations (3.20) and (3.21) can be simplified into:

$$p = u_d^f i_d^c \tag{3.22}$$

$$q = -u_d^f i_q^c \tag{3.23}$$

As shown in equations (3.22) and (3.23) the d-component of the current, i_d^c, denotes the active current and is directly related to the active power whereas the q-component, i_q^c, denotes the reactive current and depends on the reactive power. Thus, there is a nonexistence coupling between the active and reactive power nor the current. For this reason, two different outer controllers are designed:

- DC voltage controller: active power and the DC voltage of the HVDC link are related as shown in the equations of the AVM presented in Section 3.3. For Onshore converters, a DC controller instead of an active power controller is implemented to avoid a rise in the DC voltage of the link in case of power imbalance.

- Reactive power controller: maintains the reactive power at the filter bus at a constant reference value.

Both control loops are illustrated in Figure 3.3.

Outer DC voltage Controller

The DC voltage controller of the onshore converter consists of a $i_ac - V$ droop with PI controller constituted by two control loops. First a droop control strategy on the AC current flowing from the converter to the filter bus, i_d^c is implemented. The result of this operation is then added as an input signal to a DC voltage droop with a PI controller obtaining the current reference value, $i_d^{c,*}$. The equations defining this control approach are given:

$$\Delta u_{droop} = k_{droop,dc} \cdot (i_d^{c,ref} - i_d^c) \tag{3.24}$$

$$i_d^{c,*} = \left(k_{p,dc}^g + \frac{k_{i,dc}^g}{s}\right)\left[\Delta u_{droop} + u_{dc} - u_{dc}^{ref}\right] \tag{3.25}$$

Where Δu_{droop} and $k_{droop,dc}$ are the output and the droop gain of the first control loop and $k_{p,dc}^g$ and $k_{i,dc}^g$ are the proportional and the integral gains of the PI controller. $i_d^{c,ref}$ is the reference AC current value while u_{dc}^{ref} and u_{dc} are the reference and instantaneous DC voltages.

Outer reactive power controller

The outer reactive power controller adjusts the reactive power, q, to its reference value, q^{ref}, using a PI controller. The reactive controller equation is formulated by:

$$i_q^{c,*} = \left(k_{p,q}^g + \frac{k_{i,q}^g}{s}\right)\left(q_{ref} - q\right) \tag{3.26}$$

Here $k_{p,q}^g$ and $k_{i,q}^g$ are the proportional and integral gains of the reactive PI controller.

3.4.2 Wind Turbine Grid Side Converters

The Wind Turbine Aggregated model including the control scheme is presented in Figure 3.5. As mentioned previously the WT-MSC and the wind turbine dynamics are represented by a controlled current source in the aggregated model. Further, these types of VSC converter substations include a transformer that steps up the voltage from each wind turbine to the collector bus level e.g. from 0.9 kV to 33 kV. For the connection to the onshore AC hub, another step transformer is required to step up the voltage level to reduce transmission losses e.g. to 150 kV. Focusing on the control structure, the WT-GSC have a similar control approach as the Onshore-VSC since both of them operate in grid-following mode.

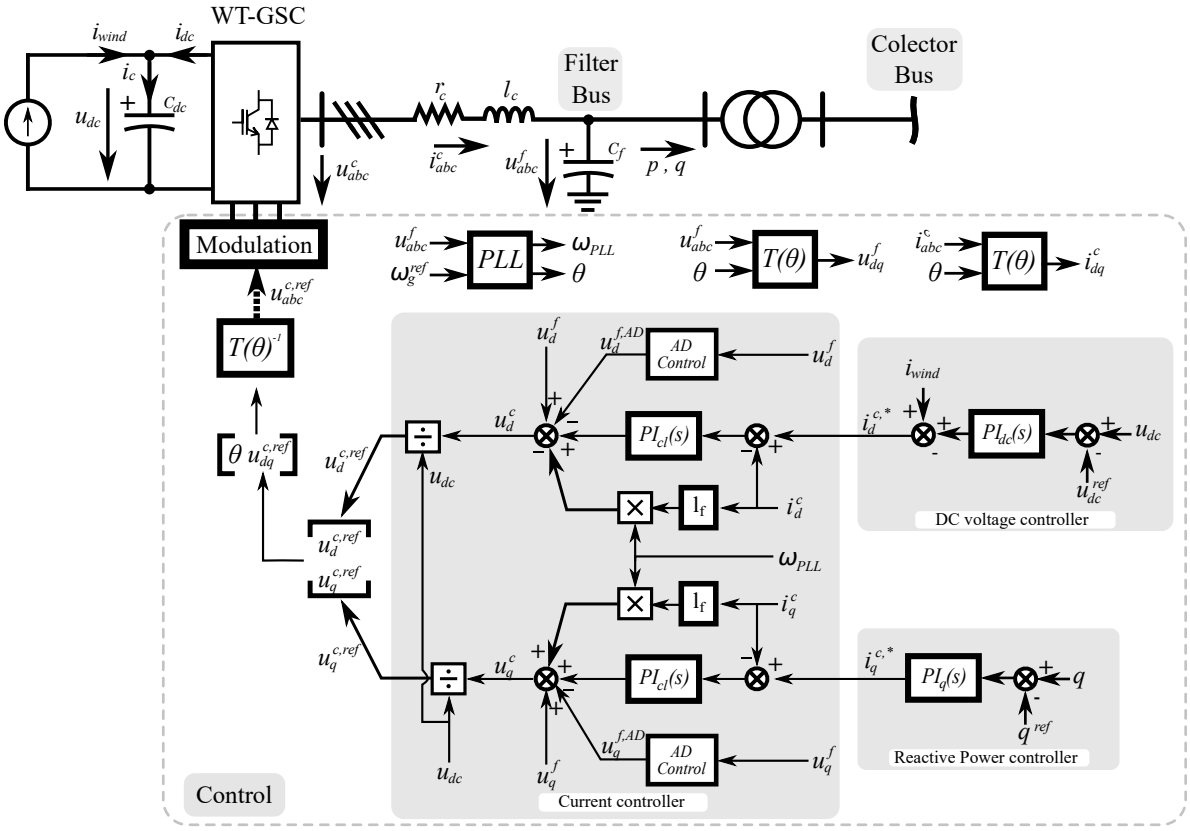

Figure 3.5: Wind Turbine-Grid Side Converter control scheme

Since both types of converters include the same control strategies for the PLL, the current controller, and the reactive power controller, previously detailed in sections 3.4.1.1, 3.4.1.2 and 3.4.1.3, their description is not included here. Nevertheless, WT-GSC do include a different control approach for the DC voltage outer controller which is described below.

3.4.2.1 Outer DC voltage Controller

WT-GSCs outer DC voltage control is based on the instant power theory which leads to equation (3.22). Moreover, if the equations of the DC side of the system in Figure 3.5 are analyzed, a relation between the DC voltage, u_{dc}, and the reference active current, $i_d^{c,*}$, is obtained. The relation between these two parameters leads to the implementation of the DC voltage controller shown in Figure 3.5. This procedure is described in the following paragraphs.

According to Kirchhoff laws, for one node the sum of the currents flowing into that node is equal to the sum of currents flowing out of it. The currents on the DC side node is described as:

$$i_{wind} + i_{dc} = i_c \tag{3.27}$$

Where i_{wind} is the current injected by the wind turbines, i_{dc} is the current flowing through the converter and i_c is the current through the DC capacitor.

At the same time, knowing that $p_{dc} = u_{dc}i_{dc}$ and that $p_{dc} = -p_{ac}$, maintaining the sign conventions from Figure 3.5, (3.27) can be reformulated as:

$$i_{wind} - \frac{u_d^c}{u_{dc}} i_d^c = i_c \tag{3.28}$$

The term $\frac{u_d^c}{u_{dc}}$ can be approximated to 1 p.u. Furthermore, from differential equation of the DC voltage capacitor (3.29) a DC voltage PI controller can be designed. This voltage controller is defined by (3.30).

$$i_c = \frac{c_{dc}}{\omega_b} \frac{du_{dc}}{dt} \tag{3.29}$$

$$i_c = \left(k_{p,q}^w + \frac{k_{i,q}^w}{s} \right) \cdot (u_{dc}^{ref} - u_{dc}) \tag{3.30}$$

In (3.29) C_{dc} corresponds to the per-unit capacitance value while ω_b is the base value of the angular frequency.

Finally, substituting (3.30) in (3.28) and taken the sign conventions into account, the outer controller expression is defined:

$$i_d^* = \left(k_{p,q}^w + \frac{k_{i,q}^w}{s} \right) \cdot (u_{dc} - u_{dc}^{ref}) + i_{wind} \tag{3.31}$$

3.5 Grid-Forming converter control

Grid-forming converters operation principle is to set or control the voltage magnitude, $u^{ref} = \sqrt{u_d^{ref^2} + u_q^{ref^2}}$, and angle, θ^{ref}, at the converter terminals. Generally, the voltage magnitude is set to 1.0 p.u. while the angle value may vary from 0 rad to 2π rad. The grid-forming mode differs from the grid-following one essentially in lacking a PLL as a mechanism of synchronization with the grid is not required. Different control strategies for grid-forming converters have been presented in the literature, from droop-based and vector control strategies to the introduction of the concept of the Virtual Synchronous Machines (VSM). Grids that include a large number of inverted based generation without dominant synchronous machines are considered weak and lack of inertia to stabilize the frequency as a grid with predominant conventional based generation would do. For this reason, the virtual synchronous machines and the concept of virtual inertia have been introduced in the literature [30].

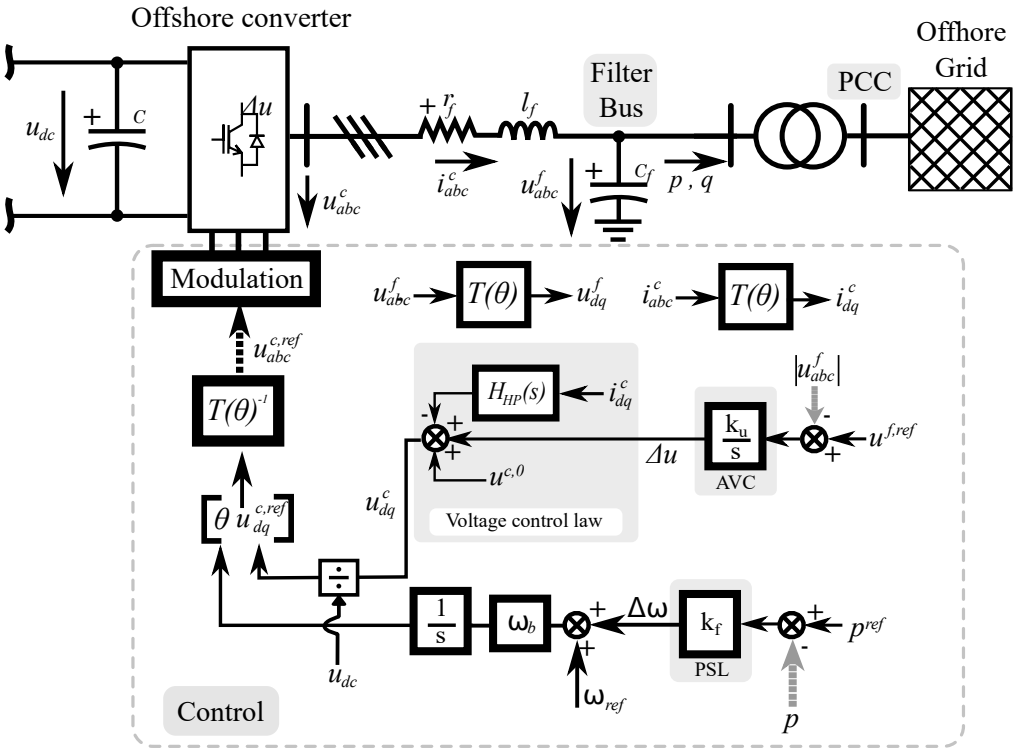

Figure 3.6: Grid Forming Converter Control Scheme

In this master thesis, the control approach for grid-forming converters is based on the control strategy described in [31]. As for the grid-following converters substations, grid-forming substations include a capacitor on the DC side, an LC filter and a transformer as shown in Figure 3.6. As in the grid-following converters, the voltage measured at the AC capacitor filter is the one used as a signal on the control strategy.

Furthermore, in the Figure 3.6, the control of the Grid Forming converter is presented. As mentioned above, there is not PLL included in the control design. Another difference with the grid-following converters relies on the lack of vector control for the converter control. This is due to the fact that the offshore converter is based on power synchronization control. This control strategy aims to replicate the behavior of the power-synchronization mechanism between two SM in which the synchronism is maintained by means of a transient power transfer. The current involved in this power transfer is generally unknown therefore a vector-current controller can not be included [32]. Further, the active power output from the VSC is controlled by the power synchronization loop (PSL) and the AC voltage by adjusting the magnitude of the voltage. Moreover, the AC voltage control is divided into two: the Alternating-Voltage Controller (AVC) and the Voltage control law. The expressions that define the control of the Offshore-VSC are explained down below.

3.5.1 Power Synchronization Loop

The Power Synchronization Loop (PSL), shown in Figure 3.6, is the control in charge of maintaining the synchronism between the VSC and the offshore AC grid. Its control law is defined by the following droop:

$$\Delta\omega_{pu} = k_f(p^{ref} - p) \tag{3.32}$$

Where p^{ref} is the reference for active power, p is the measured Power flowing to the offshore grid, k_f is the controller gain and $\Delta\omega_{pu}$ is the frequency variation and provides the synchronism.

Finally, Adding the value of $\Delta\omega_{pu}$ obtained in (3.32) to the reference ω value of the grid, ω_{ref}. Previous to obtaining the grid angle, since the quantities in the control system are in per-unit, this value must be converted in real quantities. Once the conversion is done and ω is integrated, the angle of the offshore grid, θ, is obtained. At the same time, this angle is used in the $dq0$ transform.

3.5.2 Alternating-Voltage Controller

Alternating-Voltage controller (AVC) is in charge of the control of alternating-voltage magnitude at the filter as shown in Figure 3.6. This controller is designed as an integral giving as output the change in magnitude. Its control law is described as:

$$\Delta u = \frac{k_u}{s}(u^{f,ref} - |u^f_{abc}|) \tag{3.33}$$

Here $u^{f,ref}$ is the reference voltage magnitude measured at the filter, u^f_{abc} is the measured voltage at the filter, k_u is the integral gain and Δu is the change in magnitude of the VSC reference voltage.

3.5.3 Voltage-vector Control law

Finally, a voltage-vector control law is introduced in order to damp out grid-frequency resonant poles. This law is described by:

$$u^{c,ref}_{dq} = (u^{c,0} + \Delta u) - H_{HP}(s)i^c_{dq} \tag{3.34}$$

Note that x_{dq} is expressed as $x_{dq} = x_d + jx_q$. Separating the d-components and the q-components on (3.34),the following expression is obtained:

$$\begin{aligned} u^{c,ref}_d &= (u^{c,0} + \Delta u) - H_{HP}(s)i^c_d \\ u^{c,ref}_q &= -H_{HP}(s)i^c_q \end{aligned} \tag{3.35}$$

Where $u_d^{c,ref}$ and $u_q^{c,ref}$ the output of the control system, $u^{c,0}$ the nominal voltage of the converter, i_d^c and i_q^c is the current in dq-frame flowing to the offshore grid and $H_{HP}(s)$ is a high-pass filter expressed by:

$$H_{HP}(s) = \frac{k_v s}{s + \alpha_v} \tag{3.36}$$

Here α_v sets the limits to the resonances in the AC system and k_v determines the damping effect.

CHAPTER 4

Communication based Power Control of a zero-inertia system under a DC Fault

4.1 Introduction

The offshore grid of this study interconnects two WPPs with two offshore-VSC. At the same time, these offshore-VSC transfer the generated power to two onshore grids through HVDC point-to-point connections. Even though the control strategy for each of the converters has been described in Sections 3.4 and 3.5, the power-sharing control methodology when having multiple transmission systems connected in parallel has not yet been described. This methodology is presented in this chapter.

Further, when a pole-to-pole DC fault occurs in one of the HVDC transmission lines of the system, this line is disconnected from the rest of the system, isolating the DC fault from the offshore grid. In this situation all the generated power is transferred to the other transmission line and may cause a power imbalance on the system. For this study two cases for power balance on the offshore AC hub are of main interest: a first case where the remaining transmission line is required to return to their pre-fault power values and a second case in which the new power balance is linked to the maximum power capability of the offshore-VSCs. In both cases the WPPs are required to reduce the generated power. In this chapter, the first case is studied whereas the second case is discussed in the next chapter.

For this chapter, as in [33], only the onshore-VSCs power transfer capability is limited due to maximum current rating of the converters an the maximum modulation index. However, the operational limits of the offshore-VSCs are regarded in Chapter 5.

Finally, protection systems are needed to dissipate the excess of power on the system and to isolate the DC fault from the rest of the system. These protection system are explained in this chapter.

4.2 Control Methodology

4.2.1 Active power sharing control of parallel-connected VSCs

The power sharing between the different offshore-VSC converters can either be defined by adjusting the active power set-points, p_{ref} or by changing the droop gain values, k_f. Both techniques are described in [21]. In this study the methodology of adjusting the power using set-points has been implemented, consisting of assigning different reference power values for each of the offshore-VSC converters while giving the same droop value to all. These considerations for two offshore converter system are:

$$\begin{aligned} p_{ref,1} &\neq p_{ref,2} \\ k_{f,1} = k_{f,2} = k_f &\neq 0 \end{aligned} \tag{4.1}$$

Here $p_{ref,1}$, $p_{ref,2}$, are the power reference values for the 1^{st} offshore-VSC and 2^{nd} offshore-VSC. k_f corresponds to the $\omega - p$ droop gain.

This technique allows the power transfer between two transmission lines according to the initial set-points of the offshore-VSCs which will be required further in the NSWPH project. Yet, the power transfer between onshore grids is out of the scope of this study.

4.2.2 Onshore-VSC current and voltage limitation

The power transfer through the onshore-VSC converters is limited due to the converter current ratings. If these current ratings are exceeded, the semiconductors will suffer damage. For this reason, the current of the onshore-VSC converters is limited under the following criteria:

$$i = \sqrt{{i_d}^2 + {i_q}^2} \leq i_{max} \tag{4.2}$$

This restriction is applied to the reference current signals, $i_d^{c,*}$ and $i_q^{c,*}$, used in the inner controller of the onshore-VSC converter as shown in Figure 4.1. Under both normal operation and under a DC fault, the priority is given to the active current, $i_d^{c,*}$, over the reactive current $i_q^{c,*}$. Thus, the value of the limits is given by equations (4.3) and (4.4).

$$i_d^{max} = i_{max} \tag{4.3}$$

$$i_q^{max} = \sqrt{{i_{max}}^2 - \left(\bar{i}_d^{c,*}\right)^2} \tag{4.4}$$

Further, the outer loops integrators are frozen to prevent windup during the fault as illustrated in Figure 4.2[34].

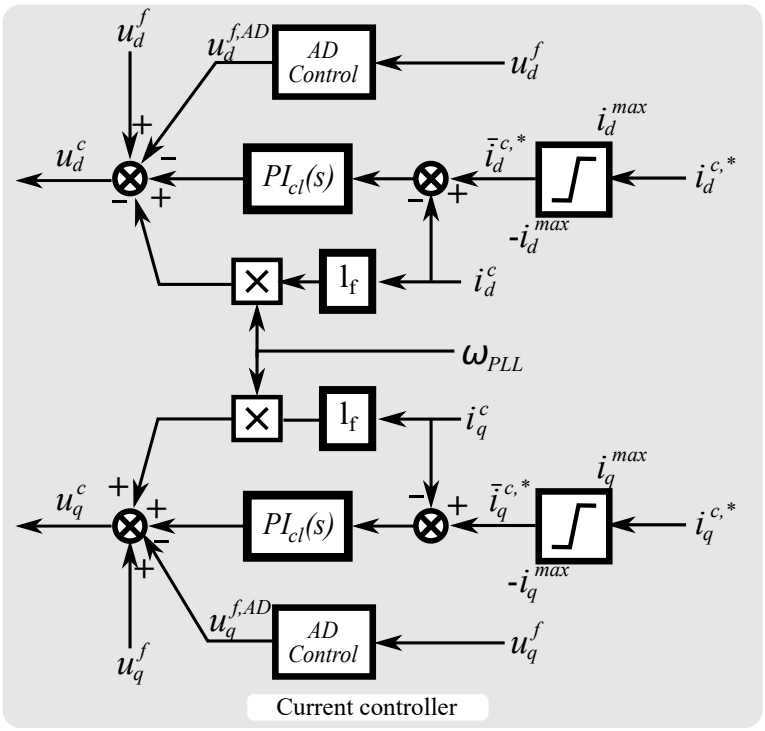

Figure 4.1: Onshore-VSC inner controller with current limitation

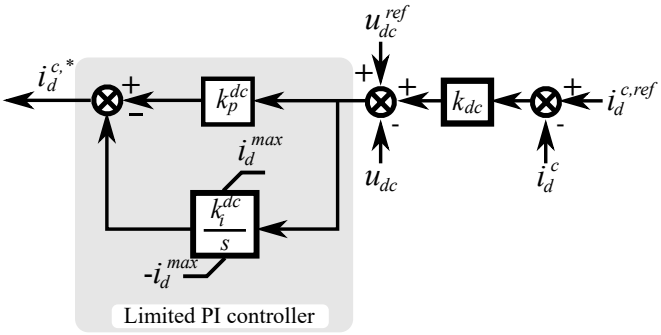

(a) Windup prevention scheme for the DC voltage controller

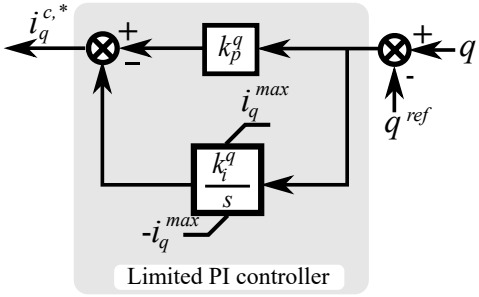

(b) Windup prevention scheme for the q controller

Figure 4.2: Windup prevention control schemes of the Onshore-VSC outer controllers

Finally, a limitation on the output voltage of the converter is introduced due to the maximum modulation index. This modulation index described by equation (3.3) is limited to 1.15 to not exceed the modulation index barrier p.u.[14]:

$$u_{ref,k} = m_k \leq 1.15 \tag{4.5}$$

Where k is the three phase index a,b,c.

4.2.3 Communication-based Control for Power reduction

The redirection of all the power generation to one transmission line due to the outage of the other transmission line of the system may originate an unbalance on the onshore network and a control strategy might be requested in order to restore the power to its pre-fault value. For that purpose, three different control approaches are defined in this section. These different control approaches are based on the same principle: using a control signal from the offshore-VSC to communicate the wind generation units to reduce the power generation.

For this study three control approaches are investigated. The description of these control proposals and their analysis are detailed in this section. First, a power reduction approach consisting on a P controller using the DC voltage of the HVDC as a control signal is introduced. Then, two more strategies are described which use a P controller and a PI controller on the frequency signal to estimate the power reduction values required for both WPPs. The control schemes of these proposals are shown in Figure 4.3.

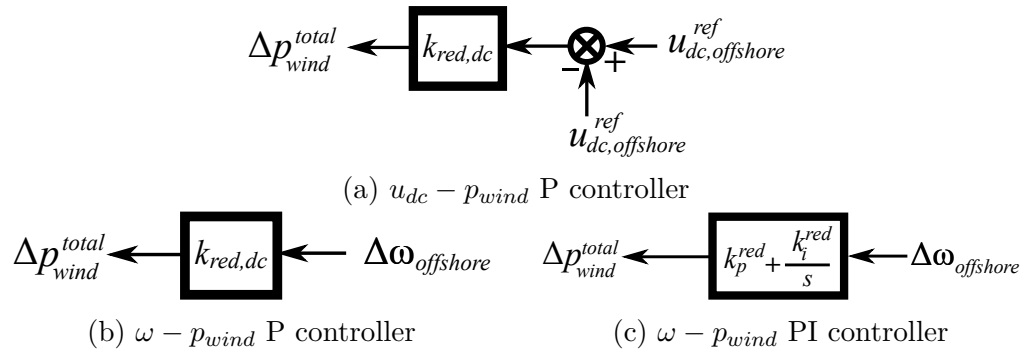

(a) $u_{dc} - p_{wind}$ P controller

(b) $\omega - p_{wind}$ P controller

(c) $\omega - p_{wind}$ PI controller

Figure 4.3: Power reduction control strategies

Finally, since these control strategies are based on communication links between the offshore-VSCs and the WPPs, a transmission delay is expected. Different transmissions delays are investigated in Section 4.5.2.2 in order to observe the system behaviour. Due to this communication delay and, in order to avoid interaction between the different control loops of the converters, the time constant of this control approach is designed to be slower than the outer and inner control loops of the converters.

4.2.3.1 P controller considering a DC voltage - Power droop $u_{dc} - p_{wind}$

When the current limit of the onshore-VSC is reached, the power that can not be transmitted to the onshore grid is stored in the DC capacitors of the HVDC link. Consequently, the voltage of the HVDC link increases. For short faults, this excess of power can be dissipated by using DC choppers whereas for longer faults such as the disconnection of a line an additional controller for power reduction might be required [35]. Under these considerations, a first control approach for the power reduction is defined:

$$\Delta p_{offshore-VSC} = k_{red,dc}(u_{dc} - u_{dc}^{ref}) \tag{4.6}$$

Where k_{red} is the controller gain and u_{dc}^{ref} and u_{dc} are the reference and measured DC voltage at the onshore-VSC station capacitor. $\Delta p_{offshore-VSC}$ corresponds to the p.u. offshore AC power variation flowing into the remaining offshore-VSCs.

Further, neglecting the AC transmission losses, the power variation of the offshore-VSC converter station is equal to the power variation requested by the wind generation system (4.7). Hence, the new power reference for each of WPPs, under the consideration of equal power reduction, is described by equation (4.8).

$$p_{wind,j} = \Delta p_{offshore-VSC} \tag{4.7}$$

$$p_{wind,j} = p_{wind,j}^{ref} - \frac{\Delta p_{offshore-VSC}}{2} \tag{4.8}$$

Here j is the index of the WT-GSCs which is comprised between: $j = 1, 2$; and $p_{wind,j}^{ref}$ is the reference power set-point for the WPPs.

Finally, combining (4.6) and (4.8) the following expression is obtained:

$$\begin{aligned} \Delta p_{wind,j} &= p_{wind,j}^{ref} - \frac{\Delta p_{offshore-VSC}}{2} \\ &= p_{wind,j}^{ref} - \frac{k_{red}(u_{dc} - u_{dc}^{ref})}{2} \end{aligned} \tag{4.9}$$

Where the $\Delta p_{offshore-VSC}$ is directly the power variation of the remaining offshore-VSC converter substation.

However, this control approach can not be implemented for this power reduction strategy due to two main reasons:

- With the conditions stated, the previous controller is only active when the onshore-VSC converter limits are reached. Thus, there is not a linear relationship between the voltage variation of the HVDC transmission link and the total active power variation. Instead, the existent relation is between the variation of power once the converter reaches its limits with the DC voltage.

- The rise of the DC voltage is not only affected by the current limitations of the onshore-VSC current limits but also by the control strategy. This outer controller is defined by equation (3.25). From this equation it is observed that a change on the AC onshore current, i_d^c, directly affects to the DC voltage of the link since the outer loop current reference, $i_d^{c,ref}$, is a fixed value set from an external reference. Once the DC fault is originated the DC voltage is going to increase due to this relation and will trigger the DC chopper if the selected droop gain is big enough. The influence of this droop on the DC voltage magnitude is analyzed through simulations in Section 4.5.2.3.

4.2.3.2 Proportional controller considering a frequency - Power droop, $\omega - p_{wind}$

When the disconnection of one of the transmission HVDC lines occurs, since the power is redirected to the other offshore-VSC converter station, the frequency of the AC offshore grid rises. This happens due to the control strategy of outer controller of the grid-forming converters described by equation (3.32). The new proposed controller is defined by:

$$\Delta p_{offshore-VSC} = k_{red,f} \Delta \omega_{offshore-VSC} \tag{4.10}$$

Where $\Delta p_{offshore-VSC}$ and $\Delta \omega_{offshore-VSC}$ are the variation of power and angular frequency of the remaining offshore-VSC converter respectively. $k_{red,f}$ is the controller gain which is equal to the inverse of the outer controller gain k_f. Furthermore, neglecting the transmission losses on the AC offshore and substituting equation (4.10) into equation (4.8), the new power generation for each WPP is obtained:

$$\begin{aligned} p_{wind,j} &= p_{wind,j}^{ref} - \frac{\Delta p_{offshore-VSC}}{2} \\ &= p_{wind,j}^{ref} - \frac{k_{red,f} \Delta \omega}{2} \end{aligned} \tag{4.11}$$

Where the $\Delta p_{offshore-VSC}$ is directly the power variation of the remaining offshore-VSC converter substation, the index j which takes the following values: $j = 1, 2$ and $p_{wind,j}$ and $p_{wind,j}^{ref}$ are the generated power and the reference power set-point of each WPP respectively.

Conversely to the first proposal, in this case, the output of the controller is linked to the variation of the offshore-VSC power variation from the initial reference set-point. Thus, with this proposal, the power reduction the pre-fault power value for this converter can be achieved. However, further studies are required to see if the power reduction value is actually close to the desired one. This analysis are performed in Section 4.5.2.1.

4.2.3.3 PI controller considering a frequency - Power, $f - p_{wind}$

For the P controllers described earlier the wind power reduction is calculated based on the assumption of no transmission losses on the AC network. However these transmission losses do exist which leads to an steady state error on the wind generation power reduction signal $\Delta p_{wind,j}$. Due to this error, the power balance is not going to be restored to the pre-fault equilibrium value. For this reason, a PI controller using the angular frequency as a control signal is now introduced as a power reduction method. This new control approach is defined by:

$$\Delta p_{offshore-VSC} = \left(k_{p,f}^{red} + \frac{k_{i,f}^{red}}{s}\right)\Delta\omega_{offshore-VSC} \tag{4.12}$$

Where $k_{p,f}^{red}$ and $k_{i,f}^{red}$ are the proportional and integral gains of the power reduction controller, $\omega_{offshore-VSC}$ corresponds to the frequency of the offshore grid and $\Delta p_{offshore-VSC}$ is the power reduction applied to the wind turbines.

Finally, the new power generation for each WPP, $p_{wind,j}$, is:

$$p_{wind,j} = p_{wind,j}^{ref} - \frac{\left(k_{p,f}^{red} + \frac{k_{i,f}^{red}}{s}\right)\Delta\omega_{offshore-VSC}}{2} \tag{4.13}$$

For the same reason as for the $\omega - p_{wind}$ P controller, this strategy is able to estimate the desired power reduction value. Further, this control is analyzed in Section 4.5.2.1 .

4.3 Protection systems

Two protection grid protection systems are described in this section. AC breakers are required when a DC fault occurs to isolate it from the rest of the system while DC choppers are used when over-voltages appear in one of the HVDC links due to an excess of power.

4.3.1 AC breakers and converter blocking

For simplicity, as in [36], only the circuit breaker fault interruption is simulated instead of a real converter blocking. Thus, two ACCB located at the AC sides of the fault-affected converters open 50 ms after the fault occurs. Finally, even though the blocking of the converters is not included, once the AC breakers are opened, the reference values for the converters are brought to zero to avoid the currents from the DC side to keep increasing.

4.3.2 DC Choppers

Chopper controlled resistors are used to dissipate the excess of power on the DC link. Consequently, they limit the DC voltage rise within safe levels [37]. In this work, a DC chopper is added near the onshore-VSC converter to dissipate the excess of power a when the DC voltage rises above a specific value. This protection system is required as the communication based control is not quick enough nor the wind turbines can decrease drastically the power generated. Further, this device is modelled as an IGBT with an anti-parallel diode as a switching device connected in series with a resistance. The size of this resistance is estimated by:

$$r_{chop} = \frac{(u_{dc,rated})^2}{p_{rated}} \tag{4.14}$$

The chopper is activated using an hysteresis control strategy in which the lower limit is set 1.01 p.u. and the upper limit is considered of 1.02 p.u. depending on the test case.

4.4 Test system

A test system is set up to validate the control methodologies described in this chapter with a focus on the proposed power reduction control. The test system, including the different voltage levels, is represented in Figure 4.4. The electrical parameters of the system are presented in Section 4.4.1.

Furthermore, WPPA and WPPB are modelled using the aggregated model shown in Figure 4.5. These aggregated models are described in [22] and neglect the collector system of the WPPs. Both wind farms aggregated models have an equal rated power generation of 63 MVA for case studies I, II, III and of 94.5 MVA for case study IV. Moreover, the DC cables are modelled using a Π equivalent while the offshore AC cables are modelled using the Γ Section equivalent [38]. Finally, regarding the onshore AC networks, these are modelled using a Thévenin equivalent composed by a three-phase voltage source and a series impedance.

Finally, the control parameters considered for the simulations are described in Section 4.4.1.

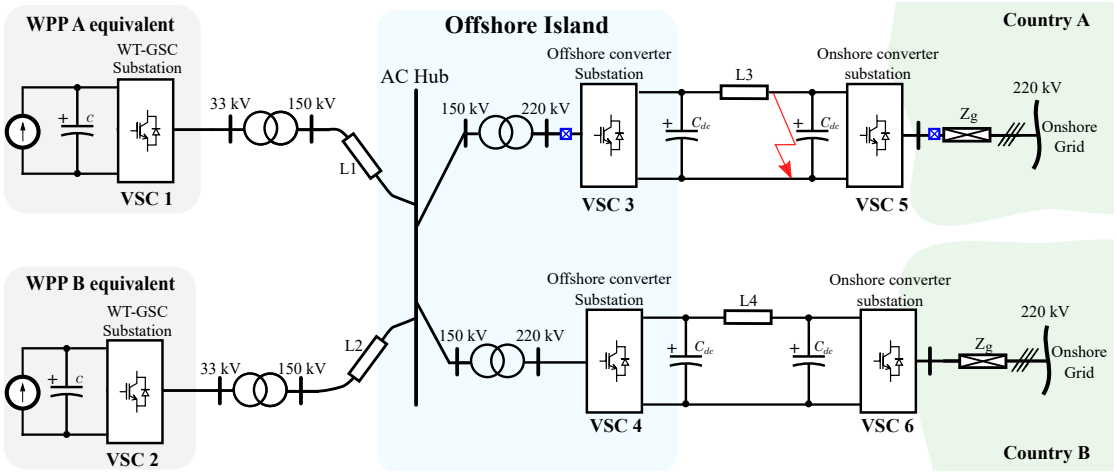

Figure 4.4: Electrical layout of the study system

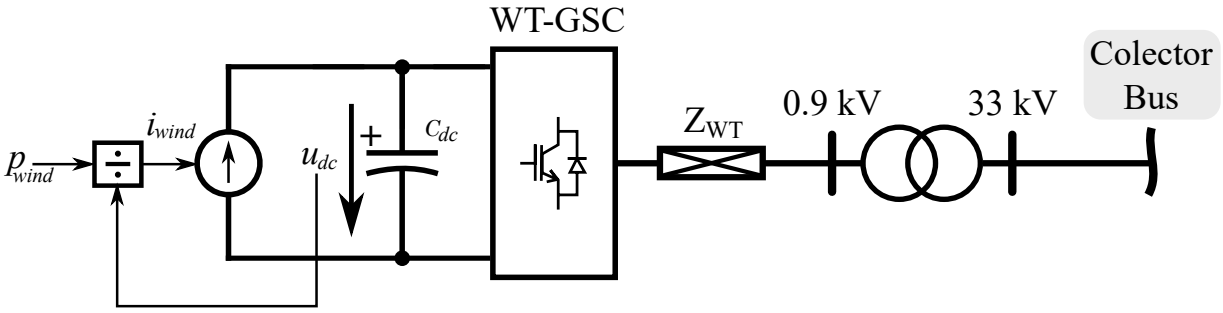

Figure 4.5: Aggregated model of the PMSG Full converter wind turbine

4.4.1 System Parameters

The parameters of the system used in the simulations are presented in this subsection. First, the electrical parameters of the system are presented. Next, the control parameters are listed.

4.4.2 Electrical Parameters

The electrical parameters of the system are listed in tables 4.1, 4.2, 4.3, 4.4 as follows:

- **Onshore grid**: the parameters for the Thévenin equivalent AC onshore grid are shown in table 4.1. These values have been extracted from [26] and [39].

- **Onshore-VSCs, Offshore-VSCs, HVDC lines**: these two converters are sized equal in the system. Further, their electrical parameters are listed in table 4.2 and are extracted from [26]. However, in this study, the rated power of the converters is 112 MVA. The maximum value for the current has been extracted from [31].

- **Offshore VSC and HV cables and Power transformers**: the values for the cable parameters of the offshore 150 kV grid are taken from as [21]. The transformer parameters have also been approximated from the values given in [21]. These values are listed in 4.3.

- **Wind Generation, WT-GSCs and DC link values**: the parameters of the wind generation system are listed in table 4.4. The rated voltage and power values and the transformer parameters, are derived from [21]. However, the p.u. values for the LC filter are extracted from [26] and [39]. The DC link capacitance has been derived from equation (4.15) considering a time constant, τ, of 5 ms [40].

$$C_{dc} = \frac{2\tau S_{c,w}}{U_{dc}^2} \tag{4.15}$$

Parameter	**Value**	**unit**
Rated Voltage, $V_{LL,RMS}$	220	kV
Grid voltage, u_g	1	p.u.
Grid inductance,V_g	0.2	p.u.
Grid resistance, r_g	0.01	p.u.
Grid frequency, f	50	Hz

Table 4.1: Onshore grid parameters

Parameter	Value	unit
VSC converters		
Rated Power, S_c	500	MVA
Rated AC Voltage, U_{HV}	220	kV
Rated DC voltage, U_{dc}	400	kV
Equivalent DC Capacitor, c^c_{dc}	150	μF
Filter resistance, r_f	0.003	p.u.
Filter inductance, l_f	0.08	p.u.
Filter capacitance, c_f	0.2	p.u.
Maximum current, i_max	1.08	p.u.
HVDC Lines		
Cable resistance, R_{dc}	0.011	Ω/km
Cable inductance, L_{dc}	2.615	mH/km
Cable capacitance, C_{dc}	0.1908	μF/km
L3 length	200	km
L4 length	200	km

Table 4.2: Onshore-VSC and Offshore-VSC parameters and HVDC lines

Parameter	Value	unit
HV Cable 150 kV		
Rated AC Voltage, U_{MV}	150	kV
Cable resistance, R_{ac}	0.06	Ω/km
Cable inductance, L_{ac}	0.44	mH/km
Cable capacitance, C_{ac}	0.14	μF/km
Cable length WPP1 to Offshore hub AC, L1	25	km
Cable length WPP2 to Offshore AC hub, L2	25	km
Transformer 33/150 kV		
Transformer Resistance, r_{tr1}	0.12	%
Transformer Inductance l_{tr1}	2	%
Transformer 150/220 kV		
Transformer Resistance, r_{tr2}	0.12	%
Transformer Inductance l_{tr2}	2	%

Table 4.3: AC cables parameters and transformers parameters

Parameter	Value	unit
Rated Power, $S_{c,w}$	6.3	MVA
Rated AC Voltage, U_{ac}	0.9	kV
Rated DC voltage, U_{dc}	2	kV
Equivalent DC Capacitor, c^c_{dc}	16	mF
Transformer Resistance, r_{tr}	0.8	%
Transformer Inductance l_{tr}	6	%
Filter resistance, r_f	0.003	p.u.
Filter inductance, l_f	0.08	p.u.
Filter capacitance, c_f	0.2	p.u.

Table 4.4: WT-GSCs parameters

4.4.3 Control Parameters

The different values for the control parameters used in Onshore-VSCs, Offshore-VSCs and WT-GSCs are listed down below in tables 4.5, 4.6 and 4.7 respectively. These values are tuned using a trial and error method in order to obtain a good dynamic performance as in [33]. As stated before, each pair of VSC is considered equal hence their control parameters are the same. The control parameters for the power reduction controllers are listed in the following Section together with the droop gain of the outer controller of the onshore-VSCs, k^g_{dc}.

Furthermore, the active power measured signal is filtered through a LPF which time constant is included in 4.6. The power synchronization droop value is small to limit the frequency rise of the offshore grid.

Parameter	**Value**	**unit**
PLL		
filter cut off frequency, $\omega^g_{LP,PLL}$	500	p.u.
Proportional gain PLL controller, $k^g_{p,pll}$	0.0844	p.u.
Integral gain PLL controller, $k^g_{i,pll}$	4.6908	p.u.
Inner loop		
Proportional gain current controller, $k^g_{p,cl}$	1.2732	p.u.
Integral gain current controller, $k^g_{i,cl}$	14.25	p.u.
Active damping gain, k^g_{ad}	0.5	p.u.
u_{dc} **outer loop**		
Considered Current droop gain controller k^g_{dc}	0.0 / 0.025 / 0.55 / 0.2	p.u.
Proportional gain u_{dc} controller, $k^g_{p,dc}$	1.0885	p.u.
Integral gain u_{dc} controller, $k^g_{i,dc}$	590.93	p.u.
q outer loop		
Proportional gain reactive power controller, $k^g_{p,q}$	0.01	p.u.
Integral gain reactive power controller, $k^g_{i,q}$	897.67	p.u.

Table 4.5: Control Parameters of the Onshore-VSC Converters

Parameter	**Value**	**unit**
Power Synchronization loop		
PSL Droop gain, k_f	0.002	p.u.
Power measurement filter time constant, τ_p	40	ms
Alternating-Voltage controller		
AVC droop gain, k_u	30	p.u.
Voltage-Vector Control Law		
High pass filter k_v	0.2	p.u.
High pass filter α_v	70	p.u.

Table 4.6: Control Parameters of the Offshore-VSC Converters

Previous to the simulation, a Power flow is performed on the study system with the wind generation values of each WPP as an input obtaining the initial values for the currents, power and voltages of the system that are used as signals in the control strategies. Moreover, the eigenvalues of the system are calculated from the small-signal model of the system to check the stability of the system.

Parameter	**Value**	**unit**
PLL		
filter cut off frequency, $\omega^g_{LP,PLL}$	50	p.u.
Proportional gain PLL controller, $k^g_{p,pll}$	0.0084	p.u.
Integral gain PLL controller, $k^g_{i,pll}$	0.0469	p.u./s
Inner loop		
Proportional gain current controller, $k^g_{p,cl}$	1.2732	p.u.
Integral gain current controller, $k^g_{i,cl}$	14.25	p.u./s
Active damping gain, k^g_{ad}	0.5	p.u.
u_{dc} **outer loop**		
Proportional gain u_{dc} controller, $k^g_{p,dc}$	1.0885	p.u.
Integral gain u_{dc} controller, $k^g_{i,dc}$	590.93	p.u./s
q outer loop		
Proportional gain reactive power controller, $k^g_{p,q}$	0.01	p.u.
Integral gain reactive power controller, $k^g_{i,q}$	897.67	p.u.

Table 4.7: Control Parameters of the WT-GSCs

4.5 Case studies and Results

4.5.1 Simulation specifications and case studies

The simulation model is build in Matlab-Simulink using the Simscape Power Systems package and a simulation step of 50 mus is considered. A total time simulation of 15 s is considered. Furthermore, at t=2 s a permanent DC pole-to-pole fault is simulated near the onshore-VSC VSC-5. 50 ms after, at t=2.05 two AC breakers situated on each terminal of the transmission system open. At the same time, the reference values of the two isolated converters are set to 0 to stop the controllers to keep acting.

Three test cases are introduced in this Section in order to validate the control methodology described in this chapter:

- **Case study I**. On this first case study the two communication based control strategies proposed are compared. The parameter of this controllers are listed in table 4.8. The control parameters for each For this comparison a time delay of 200 ms is selected and a value of 0.025 p.u. is chosen as the droop gain value for the outer loop onshore-VSC converters,$k_{dc}^{VSC5,6}$.

$\omega - p_{wind}$ **P controller**		$\omega - p_{wind}$ **PI controller**	
Parameter	Value	P controller	Value
k_{red}^{ω}	$\frac{1}{k_f} = 500$	$k_{p,red}^{\omega}$	0.5
		$k_{i,red}^{\omega}$	500

Table 4.8: Case study I controllers values

- **Case study II**. Case study II studies the behaviour of the system against different time delays for the power reduction controller. The delays considered are shown in table 4.9. For this study, the frequency PI control methodology is chosen as a power reduction controller. Furthermore, $k_{dc}^{VSC5,6}$ is selected equal to 0.025 p.u.

Delay 1	20 ms
Delay 2	200 ms
Delay 3	500 ms
Delay 4	1000 ms

Table 4.9: Case II simulated communication delays

- **Case study III**. This case study analyzes the response of the onshore converter VSC-6 and the DC voltage of the HVDC link connecting VSC-4 and VSC-6 for different values of $k_{droop,dc}^{VSC5,6}$ comparing the results from the simulations with the eigenvalues of the small-signal model. The values used are listed in table 4.10. For this case study the onshore-VSC limits are disabled. Thus, these droop value are the only contributing to the DC voltage rise.

k_{dc}^1	0.2
k_{dc}^2	0.05
k_{dc}^3	0.025
k_{dc}^4	0.0

Table 4.10: Droop values used for the case study III simulations

- **Case study IV**. This last case study focuses on analyzing the behaviour of the whole system under a DC fault, implementing the control strategies and values obtained from the three previous test cases.

Finally for the first three case studies the DC chopper upper limit is considered 1.05 p.u. whereas for the last case study this limit is reduced to 1.02 p.u.

4.5.2 Results

The simulation results are displayed in this Section and are expressed in the p.u. system considering a base power of 112 MVA.

4.5.2.1 Case study I

The results obtained applying the different control power reduction methodologies are shown in Figures 4.6, 4.7, 4.8 and 4.9 where the black lines correspond to the droop-based control strategy and the grey lines represent the PI-based control strategy. Figure 4.8 shows the response of the active power flowing through the offshore converter VSC-4. It is seen that when the fault occurs the current increases since this converter is absorbing the power that was being transferred through the disconnected transmission line. At the same time, due to this rise of power, the frequency of the offshore grid increases up to 50.05 Hz approximately as shown in Figure 4.7. It is this change of frequency what triggers the power reduction strategies. In figures 4.7 and 4.8 it can be seen that by using the PI-based control strategy, this values are restored to the pre-fault quantities approximately 2 seconds after the fault is originated whereas by using the droop-based strategy the pre-fault values are not achieved.

Furthermore, in Figure 4.6 the power reduction applied to the WPPB is shown. It is noticeable that the desired power reduction, shown in red, is only achieved by using the PI-based control.

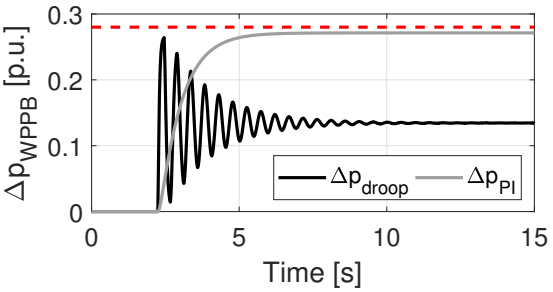

Figure 4.6: WPPB wind generation power reduction

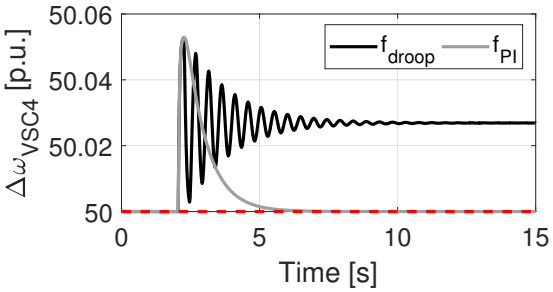

Figure 4.7: Offshore AC grid frequency measured on VSC-4 terminals

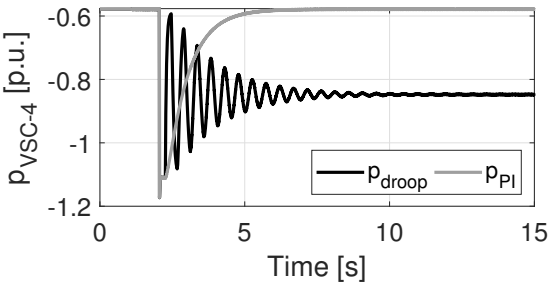

Figure 4.8: Offshore-VSC-4, active power transmitted

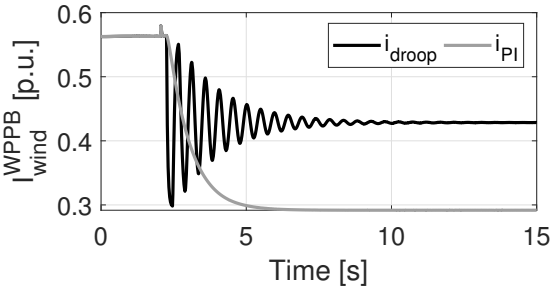

Figure 4.9: DC current injection of WPPB, i_{wind}

Hence there are some oscillations present in the droop control, other droop gains have been studied and are shown in Figure 4.10. Here it is seen that the increase of the gain generates more oscillations on the frequency response and on the whole system. As stated in [35] this may occur because the control action is too aggressive and the optimal gain selection should be done using, for example, the Nyquist criteria. Nevertheless, since the desired power reduction is not obtained with this controller, no further studies on the droop-based strategy are performed.

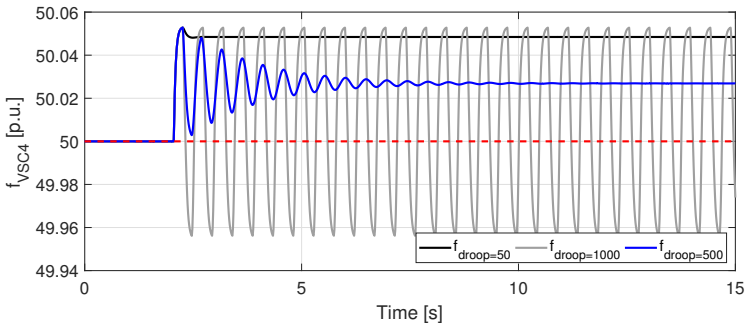

Figure 4.10: Offshore frequency for different k_{droop} values

4.5.2.2 Case study II

The results comparing different communication delays for the power reduction strategy are shown in figures 4.11, 4.12 and 4.13. Firstly, in Figure 4.11 the response of the current injection from the wind turbines of WPPB is represented. Up to a delay of 200 ms the current response can be considered of first order. For a delay equal to 500 ms this response shows a slight oscillatory behaviour, but the steady state is reached at the same time as lower delays. However for a delay of 1s, the oscillations on the system increase reaching the onshore VSC-6 operational limits as seen in figures 4.12 and 4.13. Further, in Figure 4.12 this behaviour is shown on the frequency response, limiting it around 50.3 Hz while in 4.13 the first oscillation of the active power of the offshore VSC-4 is curtailed around 1.08 p.u. Finally, to verify the onshore VSC-6 operational limits are reached, the active and reactive current injected to the grid are shown in Figure 4.14. It is seen that these limits are reached as soon as the power reduction control is applied to the wind generation system and that the active current is limited to 1.08 p.u. while the reactive current is 0 p.u.

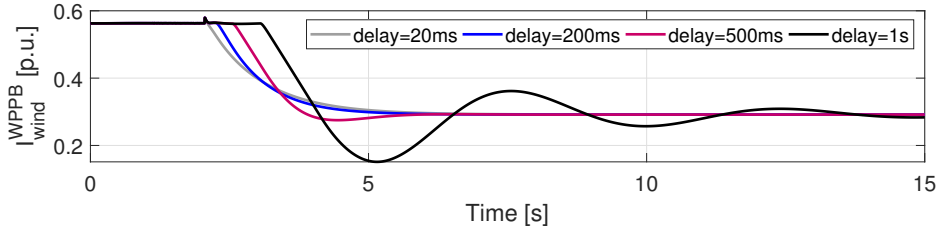

Figure 4.11: DC current injection of WPPB, i_{wind}

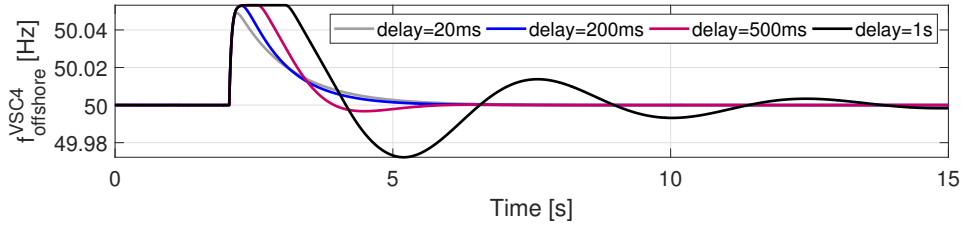

Figure 4.12: Offshore grid frequency measured in VSC-4 terminals

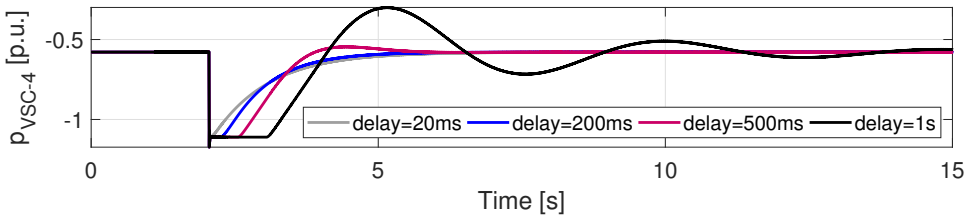

Figure 4.13: VSC-4 active power frequency measured in series reactance

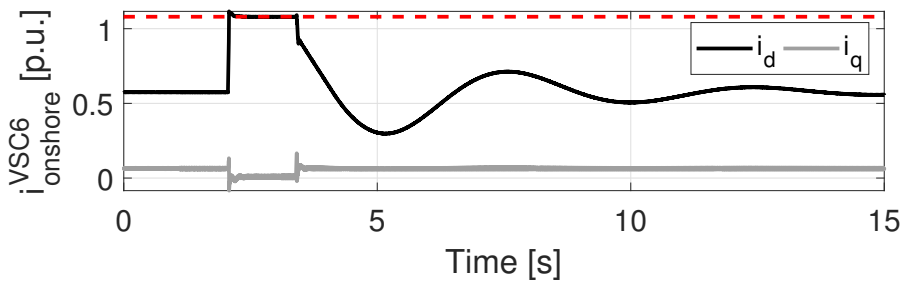

Figure 4.14: Active and reactive current measured at the VSC-6 reactance considering a delay of 1s

4.5.2.3 Case study III

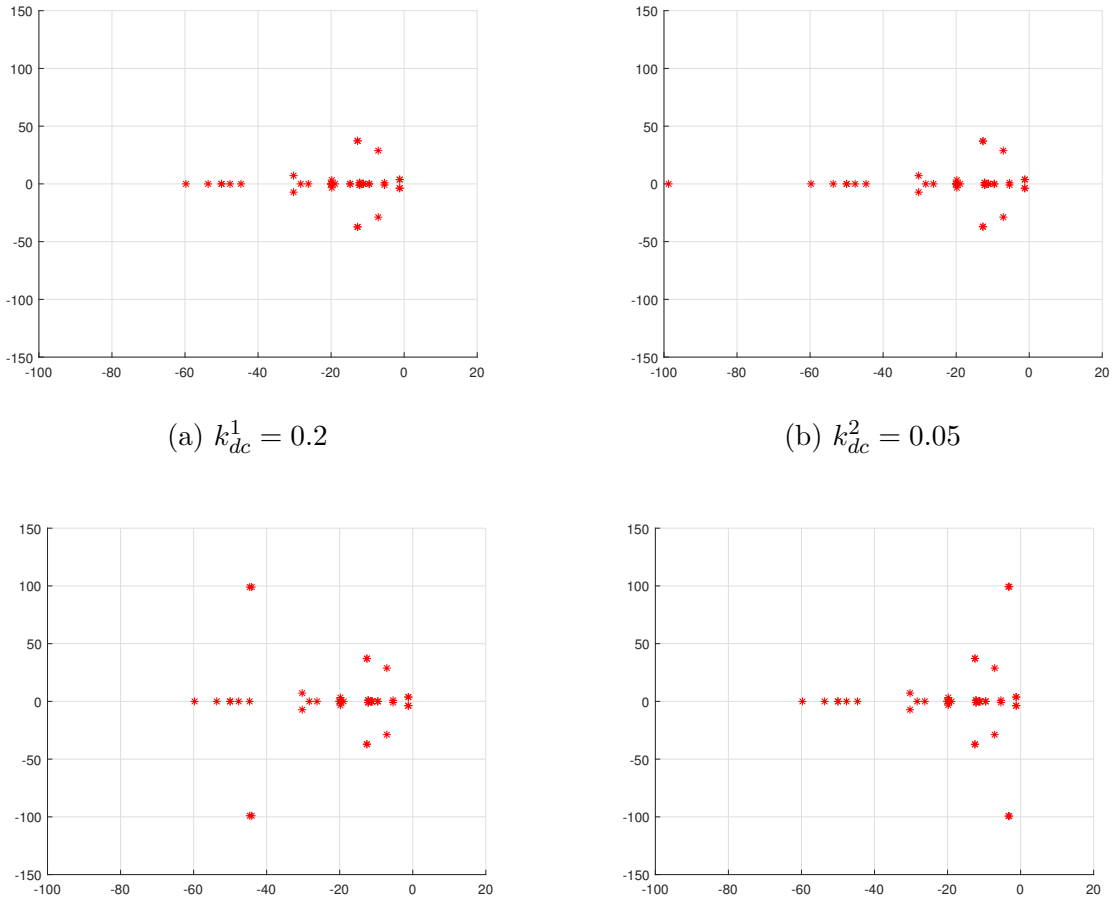

(a) $k_{dc}^1 = 0.2$

(b) $k_{dc}^2 = 0.05$

(c) $k_{dc}^3 = 0.025$

(d) $k_{dc}^4 = 0$

Figure 4.15: Representation of the system eigenvalues for different values of k_{dc}

Figure 4.15 illustrates the different eigenvalues of the system for the four current droops considered. k_{dc}^1 and k_{dc}^2 present better damped eigenvalues than k_{dc}^3 and k_{dc}^4. Further, for k_{dc}^4 the less damped poles are closer to the real axis which may lead to instabilities on the system. Thus, from the eigenvalue analysis k_{dc}^1 and k_{dc}^2 seem the best option for the system response. However, as stated before, this droop affects directly to the DC voltage rise of VSC-6 which may lead to the activation of the DC chopper. For instance, in 5.5a this activation is shown for k_{dc}^1 and consequently, the current injection to the AC onshore grid is limited to 0.8 p.u. In this scenario the power export capability of the converter is limited due to activation of the DC chopper and not to the operational limits of the converter VSC-6. Further, if this droop control is disabled, $k_{dc} = 0$, the system response presents an oscillatory behaviour and does not reach an equilibrium point. Thus, k_{dc}^1 and k_{dc}^4 are forsaken.

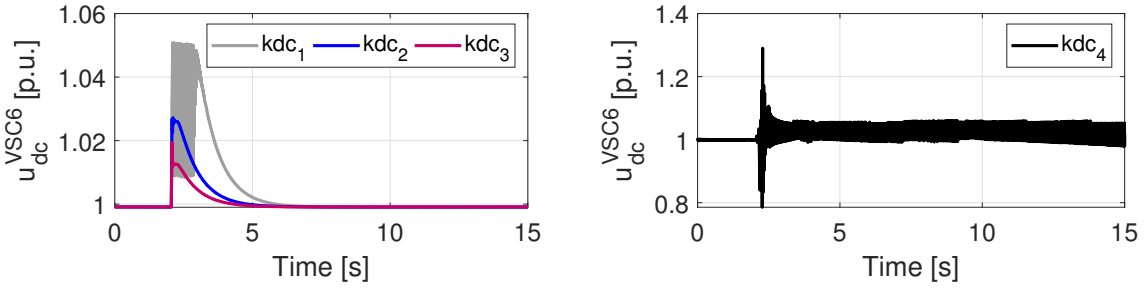

(a) $k_{dc}^1 = 0.2$, $k_{dc}^2 = 0.05$, $k_{dc}^3 = 0.025$ (b) $k_{dc}^4 = 0.0$

Figure 4.16: VSC-6 measured DC voltage

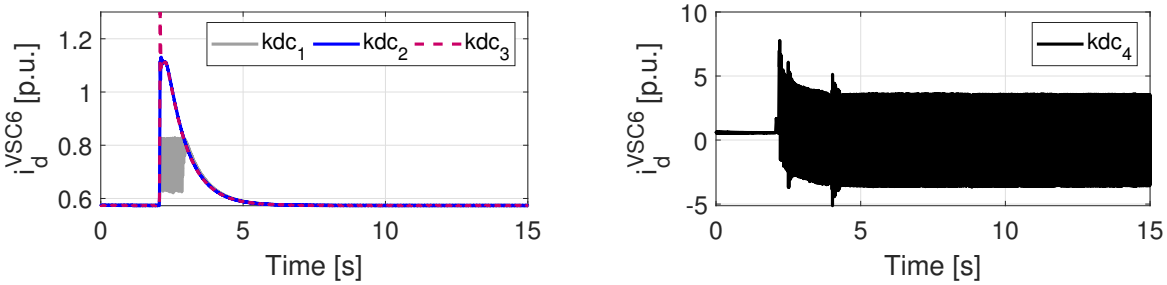

(a) $k_{dc}^1 = 0.2$, $k_{dc}^2 = 0.05$, $k_{dc}^3 = 0.025$ (b) $k_{dc}^4 = 0.0$

Figure 4.17: Active current, i_d through the series reactance VSC-6

Finally, the gains k_{dc}^2 and k_{dc}^3 are analyzed. Although with k_{dc}^2 the system presents a less oscillatory behaviour, if the activation of the DC voltage is reduced to 1.02 p.u., this gain would activate the chopper action. On the other hand, with a droop value equal to k_{dc}^3 the response of the system presents a peak when the fault is produced and the AC breakers open, but it is quickly mitigated and the pre-fault state is reached smoothly at the same time as k_{dc}^1 and k_{dc}^2. Besides, looking at the DC voltage, Figure 5.5a, the raise

using this droop value is low and does not activate the DC chopper even considering an upper limit of 1.02 p.u. Hence, k_{dc}^3 is selected as the current gain for the rest of the studies.

4.5.2.4 Case study IV

Figure 4.18 show the response on the DC components of VSC-1 for a DC fault on one of the HVDC transmission systems to shore. Figure 4.18a shows the DC voltage whereas in Figure 4.18b the DC current injection is represented. The moment the ACCB open, the DC voltage decreases for an instant, creating a small peak on the DC current. Furthermore, the communication-based control is applied after hundreds of ms reducing the wind power injection to half (0.42 p.u.).

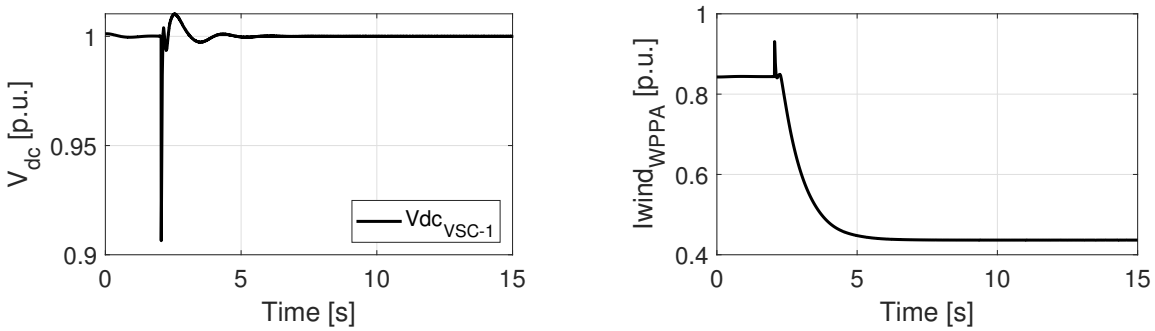

(a) Voltage of the DC link response

(b) WPPA DC current injection response

Figure 4.18: DC fault scenario response of WPPA VSC-1

Furthermore, the response of the remaining HVDC transmission system is shown in Figure 4.19. When the ACCB open 50 ms after the fault is originated, the active power of this transmission system increases as represented in 4.19a. Alongside, the onshore VSC-6 active power is limited to 1.08 p.u. due to the converter operational limits until the power reduction control is applied. On the other side, the offshore VSC-4 converter power is doubled at the fault incident. Looking into the active current of VSC-4, its value increases after the DC fault to compensate the outage of the transmission line. Furthermore, observing the active power of the offshore VSC-4, this remains above 1.5 p.u. before the control action is applied decreasing it to pre-fault value.

Regarding the AC voltage, its value remains close to 1 p.u. not exceeding the modulation index of 1.15 p.u. as shown in Figure 4.19b. Moreover, in Figure 4.19c the response of voltage of the HVDC link is illustrated. When this voltage rises up to 1.02 p.u the DC chopper activates evacuating the excess of energy until its lower limit of 1.01 p.u. is reached. Consequently there is DC voltage fluctuations until power reduction control acts. Finally, the increase of the offshore AC grid frequency when the AC breakers open and its decrease to pre-fault value are shown in Figure 4.19d.

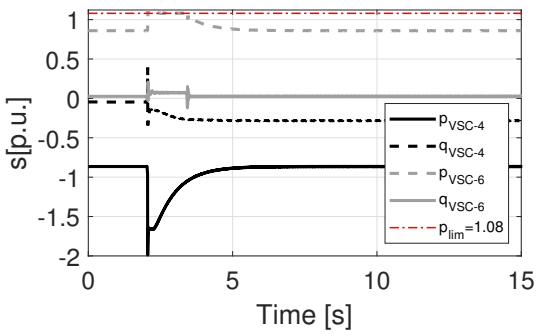

(a) Active and reactive power response

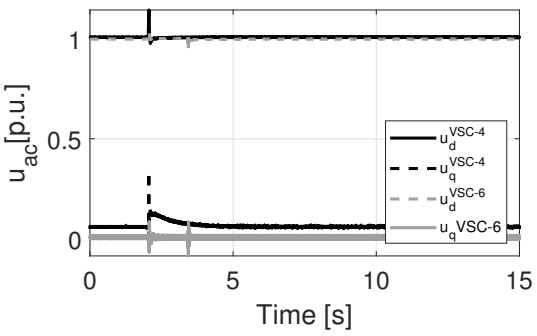

(b) voltage response

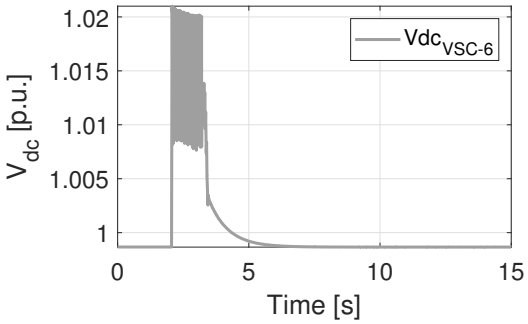

(c) DC voltage response of VSC-6

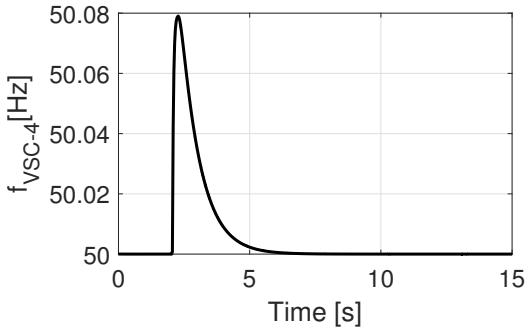

(d) offshore frequency response

Figure 4.19: DC fault scenario response of the connected HVDC transmission system involving VSC-4 and VSC-6

The response of the HVDC system in where the fault is originated is shown in Figure 4.20. When the disconnection of the transmission system occurs, the active power of converters VSC-3 and VSC-5 quickly decreases to 0 p.u. as shown in 4.20a. The reactive power of VSC-5 is not equal to zero since the power measurement is done at the grid reactance instead of the filter reactance of the converter in where this power is 0 p.u.

Finally analyzing the response of the DC components in where the DC fault is originated, it is seen in 4.20b that when the pole-to-pole fault occurs at t=3s, the voltage drastically decreases to 0 p.u. On the other hand, as shown in Figure 4.20c the current increases drastically to peak value of approximately 14.5 p.u. This value is decreased to 0 as soon as the fault is isolated opening the AC breakers and the reference values for the controller of both VSC-3 and VSC-5 are set to 0.

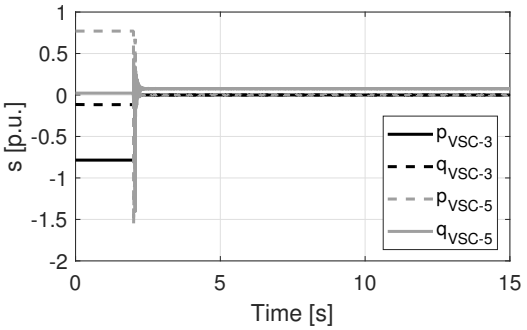

(a) Active and reactive power response

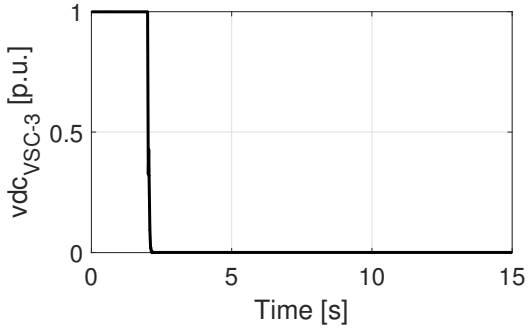

(b) DC voltage response of VSC-5

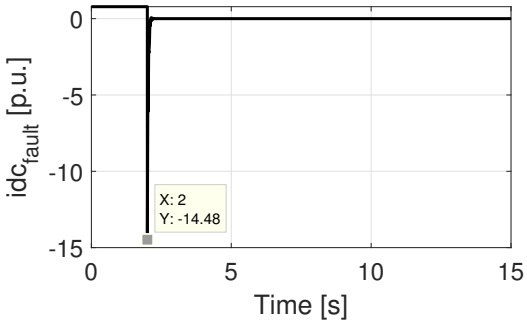

(c) DC current response

Figure 4.20: DC fault scenario response of the disconnected HVDC transmission system VSC-3 and VSC-5

CHAPTER 5

DC Fault analysis of a zero-inertia system under power constraints

This Chapter focuses on a control approach power reduction without communication and the offshore zero inertia system behavior when a permanent DC fault is originated. First, an introduction to the requirements of this non-communication control approach is presented. The current and voltage limitations regarding the converter operational limits are also described in this chapter. Furthermore, the proposed power reduction method for the wind turbines to the maximum export capability of the offshore-VSC is defined. Finally, this control strategy is validated through a nonlinear simulation of a case study system adding another case study considering the power reduction control described in Chapter 4.

5.1 Introduction

While in Chapter 4 the objective was to restore the power the remaining HVDC line after the DC fault occurrence to its pre-fault value, in this Chapter maximizing the power export is prioritized. To achieve this objective a control approach focused on the maximum power export capability of the remaining HVDC line needs to be derived.

Further, in Chapter 4 only the onshore-VSC limits were considered and it was seen that the offshore-VSC active power value reached high values for one of the simulations until the power reduction control was effective. This power value may lead to a current value above the maximum current that the IGBT can safely turn off which is typically twice as the continuous conducting current [20]. To guarantee a safe operation of the system, the offshore-VSC operational limits must also be considered.

When considering the offshore-VSC operational limits, the offshore AC network power is unbalanced as soon as the current limits of this converter are reached. Furthermore, during a power imbalance, the offshore grid causes and impact on the offshore frequency and may lead to the loss of synchronism of the power converters and the system fail. Thus, the control strategy is required to act quickly and reduce the power generation of the WPP. Under these considerations, the power reduction strategy to pre-fault values described in Chapter 4 is no longer valid. An additional control is required on the system to maintain its stability until the communication-based control . For this reason, in this thesis, the control strategy from Chapter 4 is combined with the power reduction strategy to maximum export power capability described in this chapter.

5.2 Control Methodology

5.2.1 Offshore-VSC current limitations

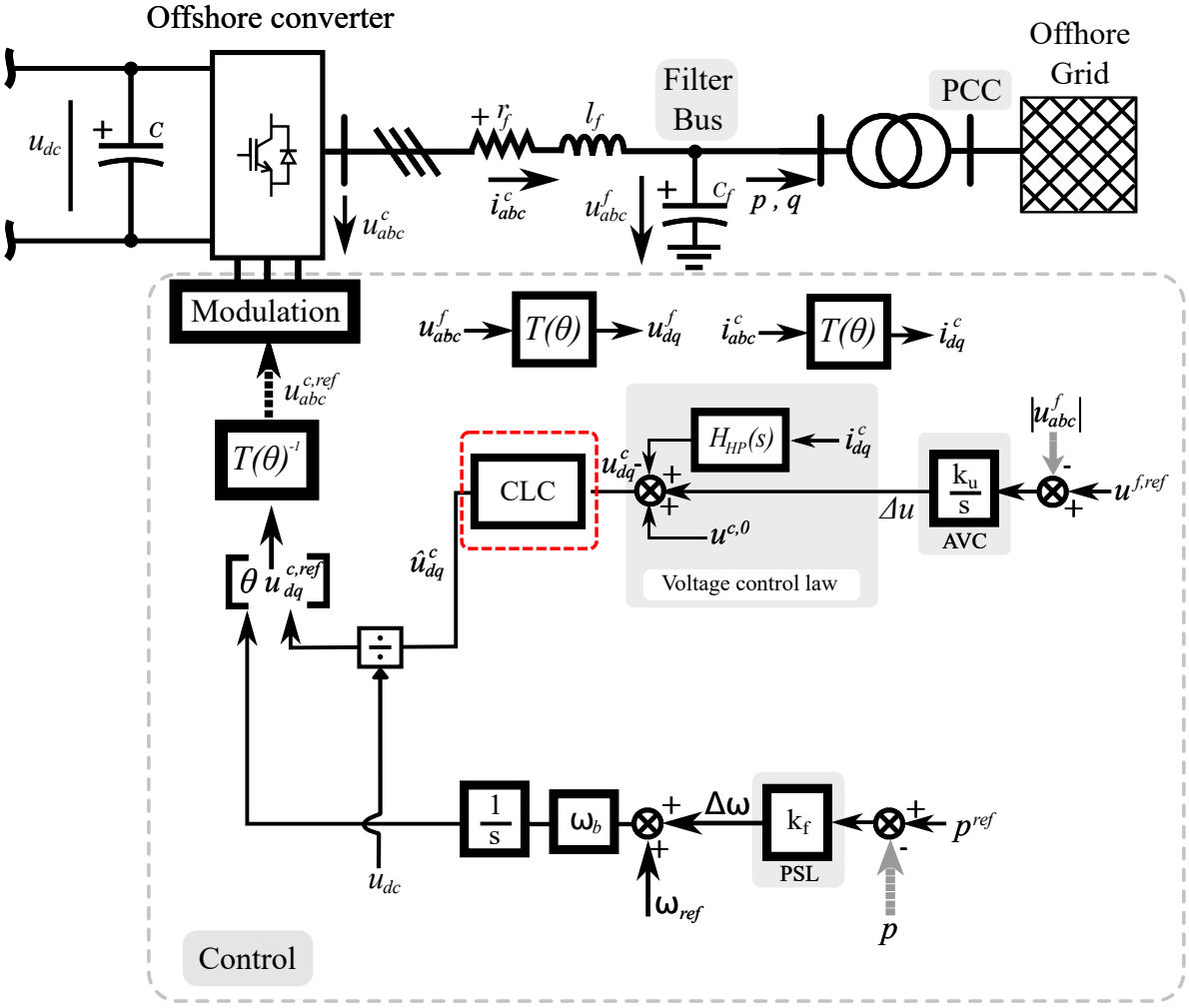

Figure 5.1: Power synchronization control of offshore-VSC including current limitation

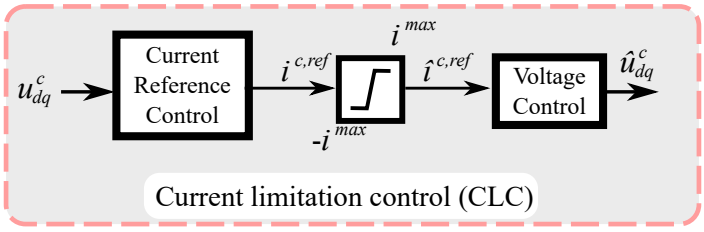

Figure 5.2: Current limitation controller

Grid-forming converters have a different control strategy that grid-following converters as described in Section 3.5. The control approach explained previously does not include a current loop nor current limitations. However, for the fault case scenario where the current rises, current limits must be included to guarantee the safety operation of the HVDC converter. These limits are included adding a Current-Limitation Controller (CLC) on the existent offshore-VSC control strategy as shown in 5.1. The design of this control is based on [31].

The CLC the block representation of this controller is illustrated in Figure 5.2. The current reference control is given by equations (5.1).

$$\begin{aligned} i_{dq}^{c,ref} &= \frac{\omega_b}{\alpha_c l_c}[u_{dq}^c - u_{dq}^f - j\omega l_f i_{dq}^c] + i_{dq}^c \\ &= \frac{\omega_b}{\alpha_c l_c}[u^{c,0} + \Delta u - H_{HP}(s) i_{dq}^c - u_{dq}^f - j\omega l_f i_{dq}^c] + i_{dq}^c \end{aligned} \tag{5.1}$$

Where $i^{c,ref}$ and i_{dq}^c are the reference and real current flowing through the series reactance of the converter respectively. α_c is the desired closed-loop bandwidth of the current control, u_{dq}^f is the voltage measured at the filter capacitance. Δu corresponds to the output of the AVC and ω and l_f are the per-unit frequency of the grid and the filter inductance of the converter.

The output of this block corresponds to the reference current which module is limited between i_{max} and $-i_{max}$. As the DC fault implies a rise in the voltage when the current limit trigger, the active current is prioritized over the reactive current. Thus, the active and reactive current maximum values, i_d^{max} and i_d^{max}, are expressed as:

$$i_d^{max} = i_{max} \tag{5.2}$$

$$i_q^{max} = \sqrt{{i_{max}}^2 - (\hat{i}_d^{c,ref})^2} \tag{5.3}$$

Where $\hat{i}_d^{c,ref}$ is the limited reference active current.

Finally, the limited current is introduced to the voltage control block to obtain the reference voltage value, $\hat{u}_{dq}^{ref}$, which is defined by the following expression:

$$\hat{u}_{dq}^{ref} = \frac{\alpha_c l_f}{\omega_b}(i_{dq}^{c,ref} - i_{dq}^c) + j\omega l_f i_{dq}^c + i_{dq}^c + u_{dq}^f \tag{5.4}$$

Note that when the current limit is not reached, the voltage reference is defined by equation (3.34).

5.2.2 Power reduction strategy to maximum export capability

During the DC fault occurrence all the power is transferred to the other offshore-VSC converter and the frequency of the offshore grid, imposed now by this remaining offshore-VSC, increases. However, the change in the frequency is slow due to the LPF introduced in the active power measurement. If used as a control signal this signal would lead to the instability of the system as soon as the power unbalanced is generated.

Another variable that can be used as a signal is the AC voltage variation. If the voltage reference at the offshore-VSC terminal is increased, the voltage of the AC offshore network increases and consequently, a voltage rise is observed in the filter capacitor of the WT-GSC systems. Hence its measurement does not include a low-pass filter, the system response is quick. Thus, the AC voltage is used as a control signal for power reduction.

Furthermore, the power reduction control needs to be quick. Thus, in this Chapter it is designed at the WPP level, becoming a local level control and not requiring a communication link between the offshore-VSC and the Wind Power Plant (WPP) which would add a delay on control signals of the system.

First, an additional control strategy on the offshore-VSC is added to step up the AC voltage of the offshore grid when the power export reaches its limits. This additional control is represented in Figure 5.3. Its output, $\Delta u^{f,ref}$ is added to the reference AC voltage magnitude becoming a new input to the Alternating-Voltage controller. The AVC is now defined by equation (5.5). This additional term, $\Delta u^{f,ref}$, is only active when the current flowing through the series reactance of the offshore-VSC is above 1 p.u. and not less than 0.9 p.u. Under this condition, the value for $\Delta u^{f,ref}$ is given by (5.6). Furthermore, a saturation block is added to $\Delta u^{f,ref}$ to avoid reaching the maximum voltage which is limited due to the maximum modulation index.

$$\Delta u = \frac{k_u}{s}(u^{f,ref} + \Delta u^{f,ref} - |u^f_{abc}|) \tag{5.5}$$

$$\Delta u^{f,ref} = k_{upr}(p^{lim}_{offshore-vsc} - p^{ref}_{wind}) \tag{5.6}$$

Where p^{ref}_{wind} is the total reference power generated by all WPPs. $p^{lim}_{offshore-vsc}$ corresponds to the maximum active power value that the offshore-VSC sytem can transfer. k_{upr} is the gain value which is chosen in order to have a $\Delta u^{f,ref}$ equal to 0.1 when the total wind generation active power is 1.2 p.u.

Finally, the new controller for active power reduction for each WPP is defined by equation (5.7) and represented in Figure 5.4.

$$p^{red}_{wind,i} = k_{upr2}(u^{f,ref}_d - u^f_d) \tag{5.7}$$

Here, k_{upr2} is the droop gain of the power reduction controller which is equal to:

$$k_{upr2} = \frac{1}{2k_{upr}} \tag{5.8}$$

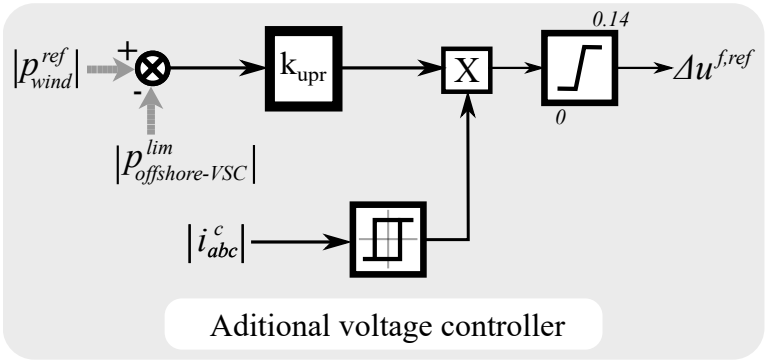

Figure 5.3: Additional power-voltage controller for offshore-VSC system

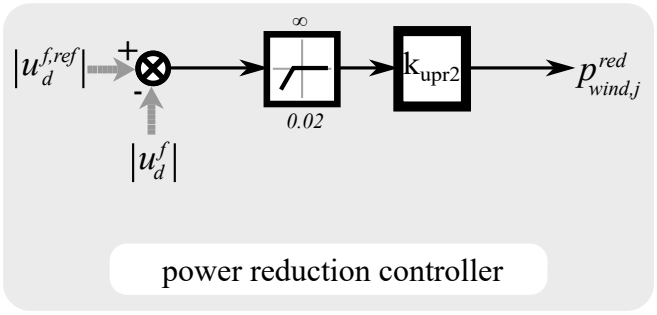

Figure 5.4: Active power reduction to maximum export capability control strategy

However, the voltage rise of the AC offshore grid is also affected by the current limitation of the offshore-VSC. To avoid triggering the modulation index, the voltage reference set-points at the filter capacitance of two WT-GSCs is set to 0.95 p.u.

5.3 Test systems

To demonstrate the performance of the proposed control methodologies as well as the control methodologies explained in the previous chapter during a permanent DC fault, two test systems are set up. Here, both systems have the same configuration and values as the test system introduced in Chapter 4, which is illustrated in Figure 4.4. Further, their electrical and control parameters are listed on the tables from Section 4.4.1. However, the control parameters required for the control strategies introduced in this chapter are listed in Table 5.1.

Parameter	**Value**	**unit**
Controller gains		
k_{upr}	0.833	p.u.
k_{upr2}	0.6	p.u.
p_{wind}^{ref}	0.6	p.u.
Limits		
Power limitation, p_{lim}	1.08	p.u.
Current limitation, i_{max}	1.08	p.u.
Hysteresis cycle upper limit of additional voltage controller	0.99	p.u.
Hysteresis cycle lower limit of additional voltage controller	0.9	p.u.

Table 5.1: Control Parameters of the power reduction controllers

Furthermore, both test systems differ in their rated power generation. For the first one, the aggregated power of each WPP is considered of 63 MVA. For the second test system, this power increased to 69.5 MVA.

5.4 Case Study and Results

5.4.1 Case studies

For this study, the simulation models are also built in Matlab-Simulink using the Simscape Power Systems package. A simulation time step of 50 mus is considered while the total simulation time is 15 s. Furthermore, at t=2 s a permanent DC pole-to-pole fault is simulated near the onshore-VSC VSC-5. 50 ms after, at t=2.05 s, the two ACCB open isolating the fault while the reference values of the isolated converters are set to 0.

Moreover, after the fault occurrence, the export power capability of the systems is reduced to 112 MVA. For the first system, this implies that the 89 % (126 MVA power generation) of the power generated can be exported through the remaining transmission line. For the second test system, the 80 % (139 MVA power generation) of the total generated power can be transferred to the onshore grid.

Finally, the two case studies analyzed are:

- **Case study I**: this first case study analyzes the behavior of the current limitations and the power reduction control for maximum power export capability presented in this chapter on both test systems.
- **Case study II**: this second case study focuses on including the communication-based power reduction control strategy defined in Chapter 4 to the model from case study I to validate the behavior of the two control strategies together. For this case study, the second test system with a total generated power of 139 MVA is considered.

5.4.2 Results

For this chapter, only the AC offshore grid and the remaining transmission line results are analyzed. The HVDC isolated system results have been already discussed in the previous chapter.

5.4.2.1 Case study I

Figure 5.5 shows the DC current injection and active voltage response of WPPB. It is seen that when the ACCB opens, there is a peak in the AC voltage and that the power reduction control acts immediately reducing the current injection. Further, it can be observed that the active voltage rises as the power reduction control activates.

The voltage rise due to the additional control for power reduction is also observed on the offshore-VSC-4 voltage response in Figure 5.6. Moreover, the response of the active power of VSC-4 is also represented in this figure. This magnitude has a peak when the ACCB open. However, this value is reduced to the power limitation value and the system is stable.

The responses of the active power and the active voltage of onshore-VSC-6 are displayed in Figure 5.7. Both components present oscillations due since the current limitation of the converter are reached.

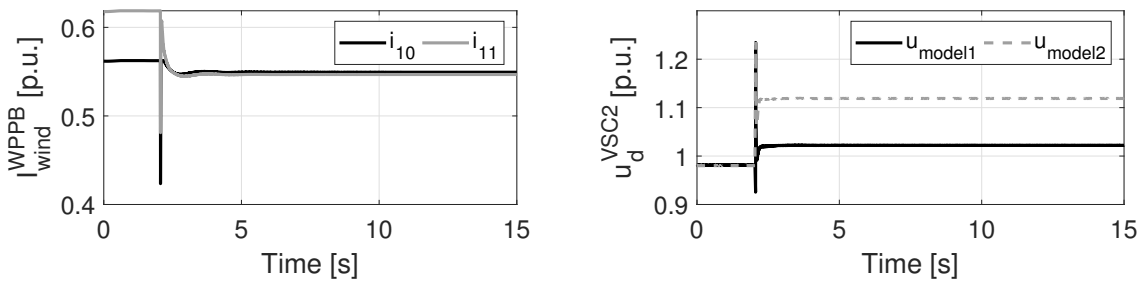

(a) DC current injection response (b) active voltage response

Figure 5.5: Case study I WPPB response of DC fault

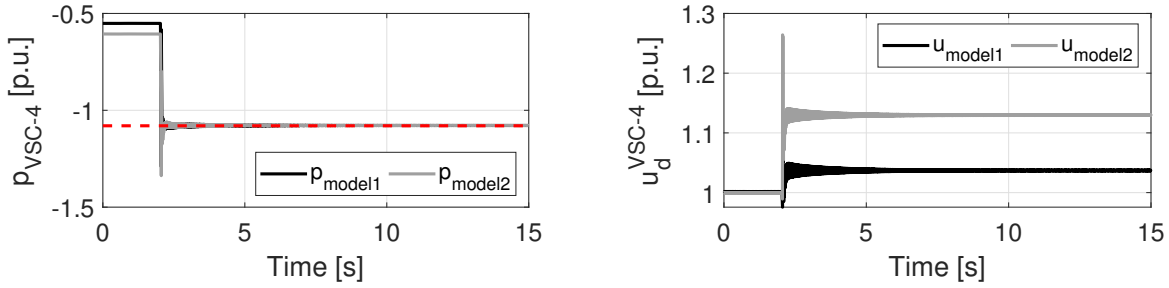

(a) active power response (b) active voltage response

Figure 5.6: Case study I VSC-4 response of DC fault

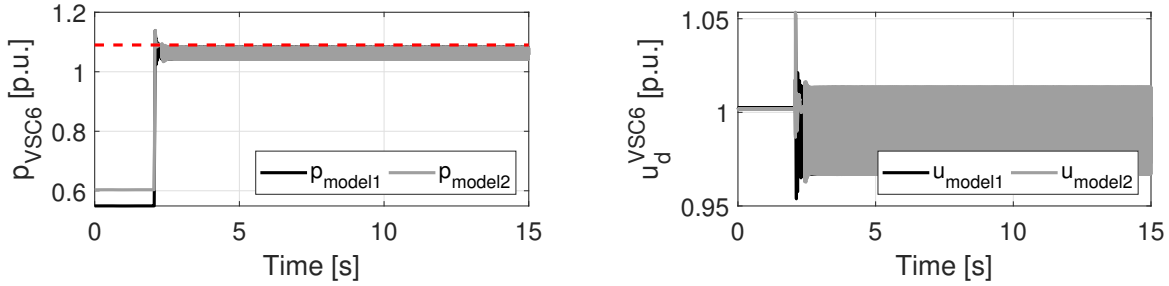

(a) active power response (b) active voltage response

Figure 5.7: Case study I VSC-6 response of DC fault

However, this power reduction control approach has limitations. First, the minimum voltage variation for the control to start acting is set to 0.02 p.u. Hence, the control strategy is not detecting lower variation values. Furthermore, the reference voltage variation, $\Delta u^{f,ref}$, depends on the difference between the total generated power and the maximum power capability of the offshore-VSC and is limited to 0.14 p.u., which limits the maximum wind generation power of each WPP to lower values around 0.65 p.u. (considering 112 MVA as a base value). Thus, further studies need to be performed and evaluated regarding this control approach.

5.4.2.2 Case study II

Figure 5.8 shows the response of the DC current injection and the active power of WPPB. By combining both power reduction strategies, the wind generation units start reducing their power injection immediately after the ACCBs open, maintaining the stability of the offshore AC grid.

The response of the active power and active voltage of the offshore-VSC-4 and the the onshore-VSC-6 are illustrated in Figure 5.9 and Figure 5.10 respectively. The active power is first reduced to the maximum export capability while the active AC voltage is increased. Then, the communication-based power reduction decreases the active power to the pre-fault values as well as decreasing the active power.

The DC voltage of the HVDC link is shown in Figure 5.11. It is seen that this voltage never rises above 1.02. Thus, the action of the DC chopper is not required.

The small oscillations observed between $t = 2.05$ s and $t = 3$ s in the different figures are due to the activation and deactivation of the power reduction control strategy for maximum export capability.

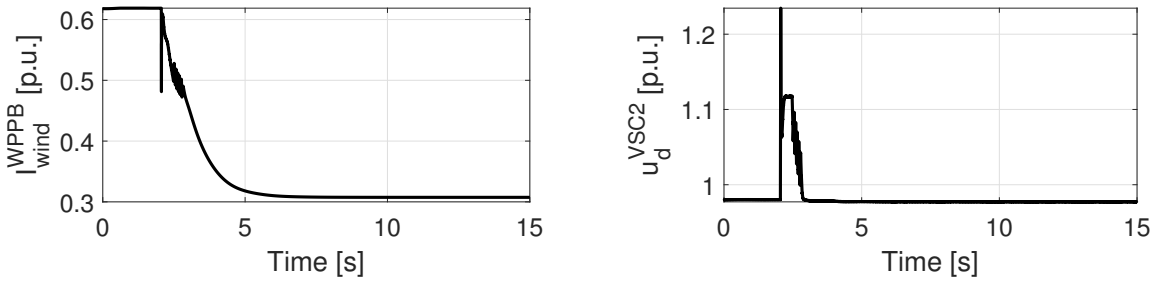

(a) DC current injection response (b) active voltage response

Figure 5.8: Case study II WPPB response of DC fault

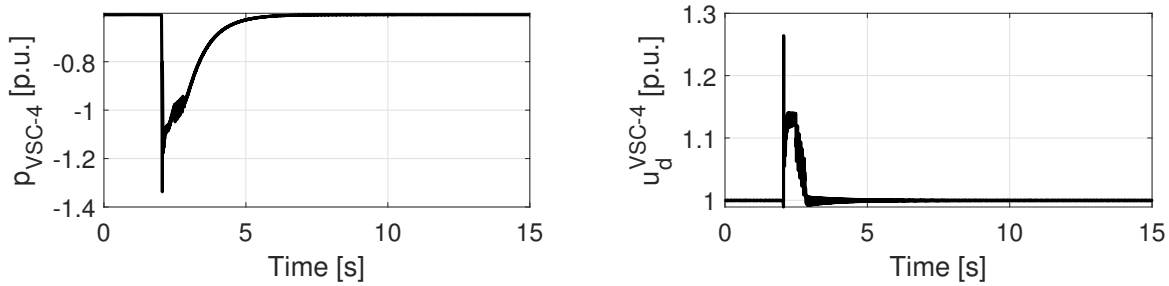

(a) active power response (b) active voltage response

Figure 5.9: Case study II VSC-4 response of DC fault

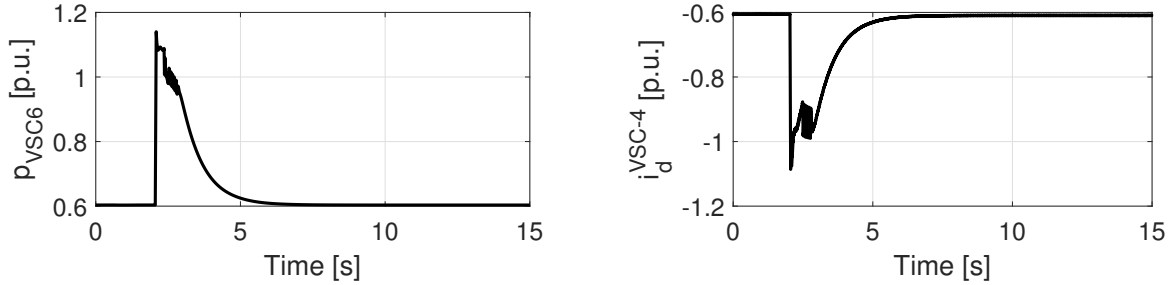

(a) active power response (b) active voltage response

Figure 5.10: Case study II VSC-6 response of DC fault

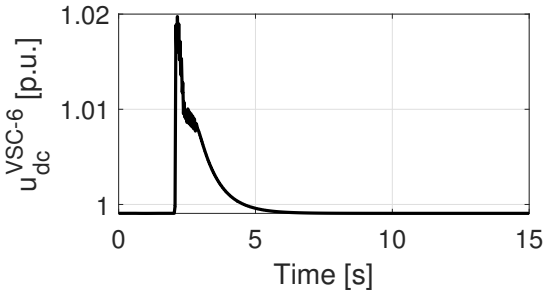

Figure 5.11: Case study II HVDC transmission line voltage response under DC fault

CHAPTER 6

Conclusion

This thesis has introduced a simplified model of an offshore AC grid for connecting two WPPs to two onshore grids through HVDC transmission lines. Moreover, the development of two control strategies for maintaining the stability of the system while reducing the power generation under a permanent pole-to-pole DC fault in one of the HVDC links have been presented.

From the **communication-based power reduction method** for restoring the HVDC link power to its pre-fault value the main conclusions have been:

- The frequency can be used as a signal for power reduction while the DC voltage of the HVDC has been discarded. Furthermore, the desired power reduction is only achieved after a few seconds by implementing a PI controller on this signal.
- The DC chopper of the HVDC may be activated due to the control action of the onshore-VSC outer controller. In this situation, the export power capability is reduced under the converter's power capability.
- By neglecting the limits of the offshore-VSC converter, in some situations, the current through this converter's IGBTs may rise above safety operation levels. For this reason, the offshore and onshore converters need to be over-sized compared to the WPP converters, being the size of the offshore converters close to two times the size of the WPP converters.

Finally, from the power reduction method to the **maximum power export capability** of the system, the conclusions have been:

- This control implementation has been verified for two different generation power values and the power through the offshore-VSC corresponds to the maximum permitted based on the limitations.
- Combining this power reduction method with the communication-based method, the system remains stable and the current through the offshore-VSC stays within safety levels after the fault occurs. Further, the power of the HVDC system is restored to the pre-fault values.
- A minimal oversize of 1.6 p.u. of the onshore and offshore converters with respect to the wind generation units achieved.

6.1 Future Work

The main Future lines of work proposed are:

- Increase the number of HVDC point to point connections from the Offshore grid to the different mainlands by 3, representing each a link to every country involved in the NSWPH.
- Update the parameter values of different elements of the system to the real system values and increase the power ratings of the VSC converters.
- Include the collector system of the Wind Power Plants in the aggregated model for more accuracy.

However work proposals include:

- Implement a DC fault with fault clearance and system restoration on the affected transmission line.
- Include Battery Energy Storage Systems (BESS) or other topologies of energy storage systems in the offshore grid.

APPENDIX A

Per Unit System

The per unit system (pu system) is a methodology broadly used in Electrical Engineering. The p.u system expresses the system real quantities as fractions of a defined base unit quantities as (A.1):

$$\text{p.u. value} = \frac{\text{value of a quantity in physical unit}}{\text{Base value in same unit}} \tag{A.1}$$

With this method, the magnitude order of the different quantities is close to one, becoming a better conditioning of numerical computations. Two different per unit systems have been used in this work, one for obtaining the p.u. values of the parameters of the electrical circuit and the other one for the measurement signals used in the different VSC controls.

A.1 Electrical circuit parameters

The conversion of the parameters of the electrical circuit to per unit magnitudes is achieved by choosing 3 base quantities. After defining this three quantities, the rest of the base values are obtained. In this case the based quantities chosen are the base power, voltage and angular frequency. In table A.1 the calculation of the p.u. value is shown. Furthermore, as a base angular frequency is chosen instead of a base time. With this choice the pu value of the reactance is equal to the p.u. value of the inductance:

$$x_{pu} = \frac{X_{real}}{Z_b} = \frac{\omega_n L_{real}}{\omega_b L_b} = \frac{L_{real}}{L_b} = l_{pu} \tag{A.2}$$

While converting in pu dynamic equations, since time is kept in seconds, a multiplying factor of $\frac{1}{\omega_b}$ will appear in front of the derivation operator.

Thus is usual for an electrical system to have different voltage levels and different power ratings, a common base power is defined. This base power commonly corresponds to the maximum rated power value of the electrical system or, otherwise, it is chosen equal to 1000 MVA. Yet, there is as much base voltages as voltage levels in the circuit. For transformers the p.u. magnitudes are referred to the high voltage level. In this work, the base values for voltage, power and angular frequency are:

$$\begin{gathered} S_b = S_{rated,max} = 112 \text{ MVA} \\ V_b = 0.9 \text{ / } 33 \text{ / } 110 \text{ / } 220 \text{ kV} \\ \omega_b = \omega_n = 2\pi 50 \text{ rad/s} \end{gathered} \tag{A.3}$$

Parameter	**Value**
Base angular frequency, ω_b	ω_n
Base Power, S_b	$S_{rated,max}$
Base Voltage,V_b	$\sqrt{\frac{2}{3}}V_{LL,RMS}$
Base Current, I_b	$\frac{S_b}{\sqrt{3}V_{LL,RMS}}$
Base impedance, Z_b	$\frac{V_b}{I_b}$
Base admittance, Y_b	$\frac{1}{Z_b}$
Base inductance, L_b	$\frac{Z_b}{\omega_b}$
Base capacitance, C_b	$\frac{Y_b}{\omega_b}$

Table A.1: Base values of the AC system

Nevertheless, the p.u. parameters listed on the different tables of Section 4.4.1 are referred to the component ratings.

Finally, referring to the DC system, its base values calculations are shown in table A.2. Here, the base power value is equal to the AC base power value while the DC base voltage corresponds to the rated DC voltage. The base values for the DC inductance and capacitance are calculated using the same base frequency as the ac system, obtaining high values.

Parameter	**Value**
Base angular frequency, ω_b	ω_n^g
Base Power, S_{bdc}	S_b
Base Voltage,V_{bdc}	V_{dc}
Base Current, I_{bdc}	S_{bdc}/V_{bdc}
Base impedance, Z_{bdc}	$\frac{V_b}{I_b}$
Base admittance, Y_{bdc}	$\frac{1}{Z_b}$
Base inductance, L_{bdc}	$\frac{Z_b}{\omega_b}$
Base capacitance, C_{bdc}	$\frac{Y_b}{\omega_b}$

Table A.2: Base values of the DC system

A.2 Control signal

For the measurement signals, inputs of the different control systems, is interesting to use the peak values of the line to line voltage and the line current as the base values as shown in table A.2. For the dc side these values are calculated as shown in A.2.

Parameter	**Value**
Base angular frequency, ω_b	ω_n
Base Voltage,V_b	$\sqrt{\frac{2}{3}}V_{LL,RMS}$
Base Current, I_b	$\sqrt{2}I_{RMS}$
Base Power, S_b	$\sqrt{3}V_{LL,RMS}\sqrt{2}I_{RMS}$

Table A.3: Base values of the AC system

APPENDIX B
Mathematical Transformations

In this appendix the Mathematical Transformations used for the implementation and control the different controllers for the different power converters are explained. First, The $dq0$ Transform is introduced, followed by the Clarke Transform.

B.1 dq0 Transform

The dq0 Transform (also known as the Park transformation) is a transformation of the vector x_{abc} in the stationary abc-reference frame into the synchronous $dq0$-reference frame vector x_{dq0} [41]. Since the $dq0$-reference frame is a projection of the phase quantities onto a two-axis rotating frame, the quantities of the x_{dq0} vector are constant and lack the oscillatory behaviour present in the vector x_{abc} . This transformation is given by (B.1):

$$\begin{bmatrix} x_d \\ x_q \\ x_0 \end{bmatrix} = T_{dq0}(\theta) \begin{bmatrix} x_a \\ x_b \\ x_c \end{bmatrix} \tag{B.1}$$

Where the transformation matrix, T_{dq0}, is defined as (B.2):

$$T_{dq0}(\theta) = \frac{2}{3} \begin{bmatrix} \cos(\theta) & \cos(\theta - 2\pi/3) & \cos(\theta + 2\pi/3) \\ -\sin(\theta) & -\sin(\theta - 2\pi/3) & -\sin(\theta + 2\pi/3) \\ \frac{1}{2} & \frac{1}{2} & \frac{1}{2} \end{bmatrix} \tag{B.2}$$

The inverse process can also be done using equation (B.3). With this operation, a transformation from the $dq0$-reference frame to the abc-reference frame is obtained. The transformation matrix, T^{-1}_{dq0} is shown in (B.4)

$$\begin{bmatrix} x_a \\ x_b \\ x_c \end{bmatrix} = T^{-1}_{dq0}(\theta) \begin{bmatrix} x_d \\ x_q \\ x_0 \end{bmatrix} \tag{B.3}$$

$$T^{-1}_{dq0}(\theta) = \begin{bmatrix} \cos(\theta) & -\sin(\omega t) & 1 \\ \cos(\theta - 2\pi/3) & -\sin(\omega t - 2\pi/3) & 1 \\ \cos(\theta + 2\pi/3) & -\sin(\omega t + 2\pi/3) & 1 \end{bmatrix} \tag{B.4}$$

This transformation can be derived applying a rotation of θ to stationary to axis reference frame obtained which results from the well-known Clarke transformation(also named alpha-beta transformation). This transformation is shown in the B.2 Clarke Transform.

B.2 Clarke Transform

The Clarke Transform (also known as the $\alpha\beta 0$ transform) is a space vector transformation of the vector x_{abc} in the stationary three-phase abc-reference frame into the stationary two-phase $\alpha\beta 0$-reference frame vector $x_{\alpha\beta 0}$ [42]. This transform is given by B.5:

$$\begin{bmatrix} x_\alpha \\ x_\beta \\ x_0 \end{bmatrix} = T_{\alpha\beta 0} \begin{bmatrix} x_a \\ x_b \\ x_c \end{bmatrix} \tag{B.5}$$

Where transformation matrix $T_{\alpha\beta 0}$ is B.6:

$$T_{\alpha\beta 0} = \frac{2}{3} \begin{bmatrix} 1 & -\frac{1}{2} & -\frac{1}{2} \\ 0 & -\frac{\sqrt{3}}{2} & \frac{\sqrt{3}}{2} \\ \frac{1}{2} & \frac{1}{2} & \frac{1}{2} \end{bmatrix} \tag{B.6}$$

As in the $dq0$ Transform, the inverse operation can be applied B.7. In this case the inverse transform matrix is B.8.

$$\begin{bmatrix} x_a \\ x_b \\ x_c \end{bmatrix} = T_{\alpha\beta 0} \begin{bmatrix} x_\alpha \\ x_\beta \\ x_0 \end{bmatrix} \tag{B.7}$$

$$T_{\alpha\beta 0}^{-1} = \begin{bmatrix} 1 & 0 & 1 \\ -\frac{1}{2} & \frac{\sqrt{3}}{2} & 1 \\ -\frac{1}{2} & -\frac{\sqrt{3}}{2} & 1 \end{bmatrix} \tag{B.8}$$

Bibliography

[1] United Nations, *Paris agreement*, Tech. Rep. December 2015.

[2] European Commission, *Political declaration on energy cooperation between the north seas countries*, Tech. Rep. 2015.

[3] The North Sea Wind Power Hub Consortium, *The vision*, 2017. [Online]. Available: `https://northseawindpowerhub.eu/wp-content/uploads/2017/11/Concept-Paper-1-The-Vision.pdf` (visited on May 12, 2019).

[4] The North Sea Wind Power Hub consortium, *Power hub as an island*, 2017. [Online]. Available: `https://northseawindpowerhub.eu/wp-content/uploads/2017/11/Concept-Paper-3-Hub-as-an-Island.pdf` (visited on May 12, 2019).

[5] The North Sea Wind Power Hub Consortium, *Modular hub and spoke*, 2017. [Online]. Available: `https://northseawindpowerhub.eu/wp-content/uploads/2017/11/Concept-Paper-2-Modular-Hub-Spoke.pdf` (visited on May 12, 2019).

[6] *MultiDC*. [Online]. Available: `http://www.multi-dc.eu/` (visited on May 12, 2019).

[7] M. Raza, E. Prieto-Araujo, and O. Gomis-Bellmunt, "Small-signal stability analysis of offshore ac network having multiple vsc-hvdc systems," *IEEE Transactions on Power Delivery*, volume 33, number 2, pages 830–839, 2017.

[8] F. Milano, F. Dörfler, G. Hug, D. J. Hill, and G. Verbič, "Foundations and challenges of low-inertia systems," in *2018 Power Systems Computation Conference (PSCC)*, IEEE, 2018, pages 1–25.

[9] G. S. Misyris, S. Chatzivasileiadis, and T. Weckesser, "Robust frequency control for varying inertia power systems," in *2018 IEEE PES Innovative Smart Grid Technologies Conference Europe (ISGT-Europe)*, October 2018, pages 1–6. DOI: `10.1109/ISGTEurope.2018.8571607`.

[10] M. Liserre, R. Cardenas, M. Molinas, and J. Rodriguez, "Overview of multi-mw wind turbines and wind parks," *IEEE Transactions on Industrial Electronics*, volume 58, number 4, pages 1081–1095, April 2011, ISSN: 0278-0046. DOI: `10.1109/TIE.2010.2103910`.

[11] T. Ackermann *et al.*, *Wind power in power systems*. Wiley Online Library, 2005, volume 140.

[12] E. Prieto Araujo, "Power converter control for offshore wind energy generation and transmission," PhD thesis, Universitat Politècnica de Catalunya, 2016.

[13] D. Zhou, F. Blaabjerg, T. Franke, M. Tønnes, and M. Lau, "Comparison of wind power converter reliability with low-speed and medium-speed permanent-magnet synchronous generators," *IEEE Transactions on Industrial Electronics*, volume 62, number 10, pages 6575–6584, October 2015, ISSN: 0278-0046. DOI: 10.1109/TIE.2015.2447502.

[14] K. Schönleber, "Control and operation of wind power plants connected to dc grids," PhD thesis, Universitat Politècnica de Catalunya, 2018.

[15] A. Egea-Alvarez, A. Junyent-Ferré, and O. Gomis-Bellmunt, "Active and reactive power control of grid connected distributed generation systems," in *Modeling and control of sustainable power systems*, Springer, 2012, pages 47–81.

[16] N. Mohan and T. M. Undeland, *Power electronics: converters, applications, and design*. John wiley & sons, 2007.

[17] A. Lesnicar and R. Marquardt, "An innovative modular multilevel converter topology suitable for a wide power range," in *2003 IEEE Bologna Power Tech Conference Proceedings,*, volume 3, Jun. 2003, 6 pp. Vol.3-. DOI: 10.1109/PTC.2003.1304403.

[18] H. Saad, J. Peralta, S. Dennetière, J. Mahseredjian, J. Jatskevich, J. A. Martinez, A. Davoudi, M. Saeedifard, V. Sood, X. Wang, J. Cano, and A. Mehrizi-Sani, "Dynamic averaged and simplified models for mmc-based hvdc transmission systems," *IEEE Transactions on Power Delivery*, volume 28, number 3, pages 1723–1730, Jul. 2013, ISSN: 0885-8977. DOI: 10.1109/TPWRD.2013.2251912.

[19] M. Abedrabbo, M. Wang, P. Tielens, F. Z. Dejene, W. Leterme, J. Beerten, and D. Van Hertem, "Impact of dc grid contingencies on ac system stability," 2017.

[20] W. Leterme and D. Van Hertem, "Classification of fault clearing strategies for hvdc grids," *Across borders-HVDC systems and markets integration: CIGRE Lund*, 2015.

[21] M. Raza, "Offshore grid control of voltage source converters for integrating offshore wind power plants," PhD thesis, Universitat Politècnica de Catalunya, 2017.

[22] J. Conroy and R. Watson, "Aggregate modelling of wind farms containing full-converter wind turbine generators with permanent magnet synchronous machines: Transient stability studies," *IET Renewable Power Generation*, volume 3, number 1, pages 39–52, 2009.

[23] J. Rocabert, A. Luna, F. Blaabjerg, and P. Rodriguez, "Control of power converters in ac microgrids," *IEEE transactions on power electronics*, volume 27, number 11, pages 4734–4749, 2012.

[24] G. Misyris, J. Mermet Guyennet., S. Chatzivasileiadis, and T. Weckesser, "Grid supporting vscs in power systems with varying inertia and short-circuit capacity," English, in *Proceedings of IEEE PES PowerTech 2019*, IEEE, 2019.

[25] H. Ouquelle, L. Dessaint, and S. Casoria, "An average value model-based design of a deadbeat controller for vsc-hvdc transmission link," in *2009 IEEE Power Energy Society General Meeting*, Jul. 2009, pages 1–6. DOI: 10.1109/PES.2009.5275748.

[26] F. Thams, R. Eriksson, and M. Molinas, "Interaction of droop control structures and its inherent effect on the power transfer limits in multiterminal vsc-hvdc," *IEEE Transactions on Power Delivery*, volume 32, number 1, pages 182–192, February 2017, ISSN: 0885-8977. DOI: 10.1109/TPWRD.2016.2600028.

[27] S. D'Arco, J. A. Suul, and M. Molinas, "Implementation and analysis of a control scheme for damping of oscillations in vsc-based hvdc grids," in *2014 16th International Power Electronics and Motion Control Conference and Exposition*, Sep. 2014, pages 586–593. DOI: 10.1109/EPEPEMC.2014.6980558.

[28] C. Bajracharya, M. Molinas, J. A. Suul, T. M. Undeland, *et al.*, "Understanding of tuning techniques of converter controllers for vsc-hvdc," in *Nordic Workshop on Power and Industrial Electronics (NORPIE/2008), June 9-11, 2008, Espoo, Finland*, Helsinki University of Technology, 2008.

[29] H. Akagi, E. H. Watanabe, and M. Aredes, *Instantaneous power theory and applications to power conditioning*. John Wiley & Sons, 2017, volume 62.

[30] S. D'Arco and J. A. Suul, "Virtual synchronous machines—classification of implementations and analysis of equivalence to droop controllers for microgrids," in *2013 IEEE Grenoble Conference*, IEEE, 2013, pages 1–7.

[31] L. Zhang, L. Harnefors, and H.-P. Nee, "Power-synchronization control of grid-connected voltage-source converters," *IEEE Transactions on Power systems*, volume 25, number 2, pages 809–820, 2009.

[32] L. Zhang, "Modeling and control of vsc-hvdc links connected to weak ac systems," PhD thesis, KTH, 2010.

[33] X. Hu, J. Liang, D. J. Rogers, and Y. Li, "Power flow and power reduction control using variable frequency of offshore ac grids," *IEEE Transactions on Power Systems*, volume 28, number 4, pages 3897–3905, 2013.

[34] L. Papangelis, M.-S. Debry, T. Prevost, P. Panciatici, and T. Van Cutsem, "Stability of a voltage source converter subject to decrease of short-circuit capacity: A case study," in *2018 Power Systems Computation Conference (PSCC)*, IEEE, 2018, pages 1–7.

[35] A. Egea-Àlvarez, M. Aragüés-Peñalba, E. Prieto-Araujo, and O. Gomis-Bellmunt, "Power reduction coordinated scheme for wind power plants connected with vsc-hvdc," *Renewable energy*, volume 107, pages 1–13, 2017.

[36] I. Erlich, A. Korai, T. Neumann, M. Koochack Zadeh, S. Vogt, C. Buchhagen, C. Rauscher, A. Menze, and J. Jung, "New control of wind turbines ensuring stable and secure operation following islanding of wind farms," *IEEE Transactions on Energy Conversion*, volume 32, number 3, pages 1263–1271, Sep. 2017, ISSN: 0885-8969. DOI: 10.1109/TEC.2017.2728703.

[37] S. K. Chaudhary, R. Teodorescu, P. Rodriguez, and P. C. Kjær, "Chopper controlled resistors in vsc-hvdc transmission for wpp with full-scale converters," in *2009 IEEE PES/IAS Conference on Sustainable Alternative Energy (SAE)*, Sep. 2009, pages 1–8. DOI: 10.1109/SAE.2009.5534882.

[38] L. P. Kunjumuhammed, B. C. Pal, C. Oates, and K. J. Dyke, "Electrical oscillations in wind farm systems: Analysis and insight based on detailed modeling," *IEEE Transactions on Sustainable Energy*, volume 7, number 1, pages 51–62, January 2016, ISSN: 1949-3029. DOI: 10.1109/TSTE.2015.2472476.

[39] S. D'Arco, G. Guidi, and J. A. Suul, "Embedded limitations and protections for droop-based control schemes with cascaded loops in the synchronous reference frame," in *2014 International Power Electronics Conference (IPEC-Hiroshima 2014 - ECCE ASIA)*, May 2014, pages 1544–1551. DOI: 10.1109/IPEC.2014.6869790.

[40] T. Kalitjuka, "Control of voltage source converters for power system applications," Master's thesis, Institutt for elkraftteknikk, 2011.

[41] R. H. Park, "Two-reaction theory of synchronous machines generalized method of analysis-part i," *Transactions of the American Institute of Electrical Engineers*, volume 48, number 3, pages 716–727, Jul. 1929, ISSN: 0096-3860. DOI: 10.1109/T-AIEE.1929.5055275.

[42] E. Clarke, *Circuit analysis of AC power systems*. Wiley, 1943, volume 1.